

Empirical color correction to MIST and PARSEC isochrones on Gaia BR–RP and G–RP with benchmark open clusters

FAN WANG,^{1,2} MIN FANG,^{1,2} XIAOTING FU,^{1,2} YANG CHEN,³ LU LI,^{4,5} XIAOYING PANG,^{6,7} ZHONGMU LI,⁸ JING TANG,⁹ WENYUAN CUI,¹⁰ HAIJUN TIAN,^{11,12} AND CHAO LIU⁹

¹*Purple Mountain Observatory, Chinese Academy of Sciences, 10 Yuanhua Road, Nanjing 210023, China*

²*University of Science and Technology of China, Hefei 230026, China*

³*School of Physics and Optoelectronic Engineering, Anhui University, 230601, Hefei, China*

⁴*Key Laboratory for Research in Galaxies and Cosmology, Shanghai Astronomical Observatory, Chinese Academy of Sciences, 80 Nandan Road, Shanghai 200030, China*

⁵*University of Chinese Academy of Sciences, No. 19A Yuquan Road, Beijing 100049, China*

⁶*Department of Physics, Xi'an Jiaotong-Liverpool University, 111 Ren'ai Road, Dushu Lake Science and Education Innovation District, Suzhou 215123, Jiangsu Province, China*

⁷*Shanghai Key Laboratory for Astrophysics, Shanghai Normal University, 100 Guilin Road, Shanghai 200234, China*

⁸*Institute of Astronomy, Dali University, Dali 671003, China*

⁹*National Astronomical Observatories, Chinese Academy of Sciences, 100101, Beijing, China*

¹⁰*College of Physics, Hebei Normal University, Shijiazhuang 050024, China*

¹¹*School of Science, Hangzhou Dianzi University, Hangzhou 310018, China*

¹²*Big Data Institute, Hangzhou Dianzi University, Hangzhou 310018, China*

ABSTRACT

Recent literature reports a color deviation between observed Gaia color-magnitude diagrams (CMDs) and theoretical model isochrone predictions, particularly in the very low-mass regime. To assess its impact on cluster age determination via isochrone fitting, we quantified the color deviations for three benchmark clusters, Hyades, Pleiades, and Praesepe, both for the Gaia color (BP–RP) and (G–RP). In general, the (G–RP) color deviations are smaller than the (BP–RP) ones. Empirical color correction functions based on these benchmarks are derived for the currently available MIST and PARSEC 1.2S isochrone models. Applying the correction functions to 31 additional open clusters and 3 moving groups results in a significantly improved alignment between the isochrones and observed CMDs. With our empirical corrections, isochrones provide age estimates consistent with literature values obtained through the spectral Lithium Depletion Boundary method, validating the effectiveness of our approach. The corresponding metallicities with PARSEC 1.2S also show a good agreement with the spectroscopic results. The empirical color correction function we present in this work offers a tool for a consistent age determination within the full mass range of stellar clusters using the isochrone fitting method.

Keywords: Open cluster; Isochrone

1. INTRODUCTION

The isochrone fitting method is commonly employed to derive star cluster parameters like age, metallicity, distance, and reddening (see e.g., Pietrinferni et al. 2004; Tognelli et al. 2011; Dotter 2016; Bressan et al. 2012; Li & Shao 2022). Cluster age, crucial for understanding formation and evolution (Soderblom et al. 2009; Galli et al. 2023), relies on both precise observa-

tional data and robust isochrone models. The Gaia mission¹ has revolutionized star cluster studies by providing high-precision photometry and astrometry (proper motion and parallax) for a vast number of stars. With this support, fitting isochrones on color-magnitude diagram (CMD) to derive the age of nearby stellar populations, including open clusters and moving groups, has become significantly more accurate than in the pre-Gaia era. Isochrones of two stellar evolutionary models are widely used in the community, MIST (MESA Isochrones & Stel-

Corresponding author: Min Fang
mfang@pmo.ac.cn

¹ <https://www.cosmos.esa.int/web/gaia>

lar Tracks, Dotter 2016; Choi et al. 2016) and PARSEC (the PAdova & TRieste Stellar Evolution Code, Bressan et al. 2012; Tang et al. 2014; Chen et al. 2014, 2015).

However, different models used in isochrone fitting introduces systematic offsets in age determinations. Bell et al. (2015) found that fitting the observed photometry of the β Pic moving group with various isochrone models (BHAC15, Dartmouth, PARSEC, Pisa) yielded age estimates ranging from 10 Myr to 20 Myr. The issue has been observed in other nearby moving groups and open clusters (e.g., Mamajek & Bell 2014; Bell et al. 2015; Kerr et al. 2022; Lee et al. 2024). The age variations with different isochrones can be attributed to the stellar models’ physics input, treatment of mixing in the stellar interior, and stellar atmosphere models used for the bolometric corrections.

No model is perfect, though. It has been discussed for a long time that, for given photometry systems or evolutionary stages, there are color discrepancies on the CMD between observations and model predictions. (see e.g., Castellani et al. 2001; Preibisch 2012; Bell et al. 2015; Kopytova et al. 2016; Siegel et al. 2019; Li et al. 2020). This is particularly conspicuous in the Gaia era due to the high precision of Gaia photometry and astrometry. In a series of papers, Brandner et al. (2023a,b,c) show that the CMDs of open clusters with Gaia DR3 photometry exhibit deviations from the MIST and PARSEC model isochrones at the low-mass range.

Modelling low mass stars is complex. Discussions in the literature (e.g., Stauffer et al. 1998; Baraffe et al. 2002; Da Rio et al. 2010; Bell et al. 2014) suggest that the observation and model deviation on CMD at the low-mass part could be a combination of factors, including the stellar interior structure and atmosphere models, especially at lower temperatures T_{eff} , as well as other factors affecting photometric data such as magnetic activity (Bell et al. 2014).

The isochrone color deviation is not unique to GaiaDR3 photometry. It is also seen with GaiaDR2 data (see isochrone fitting figures in e.g. Bossini et al. 2019) and other passbands (see e.g. Fritzewski et al. 2019). The color deviation is also considered a contributor to age differences between different studies (see e.g. Lee et al. 2022), especially for young moving groups (e.g., Feiden 2016; Naylor 2009; Herczeg & Hillenbrand 2015). Magnetic inhibition of convection in cool stars, verified by Feiden (2016); Jeffries et al. (2017), could be a possible explanation.

Color deviation can affect the determination of age and binary fraction. At the upper main sequence, the model isochrone roughly matches the actual photometric data of the star cluster. However, at the lower main

sequence, color deviation between the model isochrone and the actual photometric data leads to inconsistent age determinations based on the upper main sequence end. A bluer color of the model isochrone can also lead to an overestimation of the binary fraction. For older star clusters, the single star and binary sequences are usually distinguishable in CMDs. For example, the ridge line method can be used effectively to determine the binary fraction of the cluster. However, for young clusters, their distributions in CMDs are scattered, which makes it difficult to determine their binary fractions without correct model isochrones.

This study aims to address this issue by deriving an empirical color correction function for Gaia DR3 photometry (BP–RP) and (G–RP) using benchmark clusters with minimal extinction and high-confidence age determinations. The goal is to improve agreement between model isochrones and observed clusters for a better age determination. The Hyades, Pleiades, and Praesepe clusters serve as our benchmark targets.

The structure of the paper is outlined as follows. Section 2 describes the data and isochrone models we use in this work. Section 3 demonstrates the color deviations between the CMDs of the Hyades, Pleiades, and Praesepe clusters and model isochrones. Section 4 describes the color correction process. Section 5 verifies the validity of the color correction function using 31 clusters and 3 moving groups. Section 6 is the summary and discussions.

2. DATA AND MODELS

In this section, we briefly introduce the data and stellar isochrones we use in this work, including the GaiaDR3 (Gaia Collaboration et al. 2023) data, the MIST (Dotter 2016; Choi et al. 2016) and PARSEC 1.2S (Bressan et al. 2012; Tang et al. 2014; Chen et al. 2015) isochrone models.

2.1. Gaia DR3

The third release of the Gaia Data (DR3) (Gaia Collaboration et al. 2023) provides astrometric information for about 1.8 billion sources across the sky, along with near-mmag precision photometric data in G, G_{BP} and G_{RP} bands. The typical parallax uncertainty is 0.07 mas at $G \approx 17$ mag and 0.5 mas at $G = 20$ mag. The mean G-band photometry uncertainty is 1 mmag at $G \approx 17$ mag and 6 mmag at $G = 20$ mag. This very high precision in astrometry and photometry allows us to identify discrepancies between observations and isochrone model predictions, even when the differences are small.

The open cluster member stars we use in this work are adopted from Cantat-Gaudin et al. (2020, hereafter

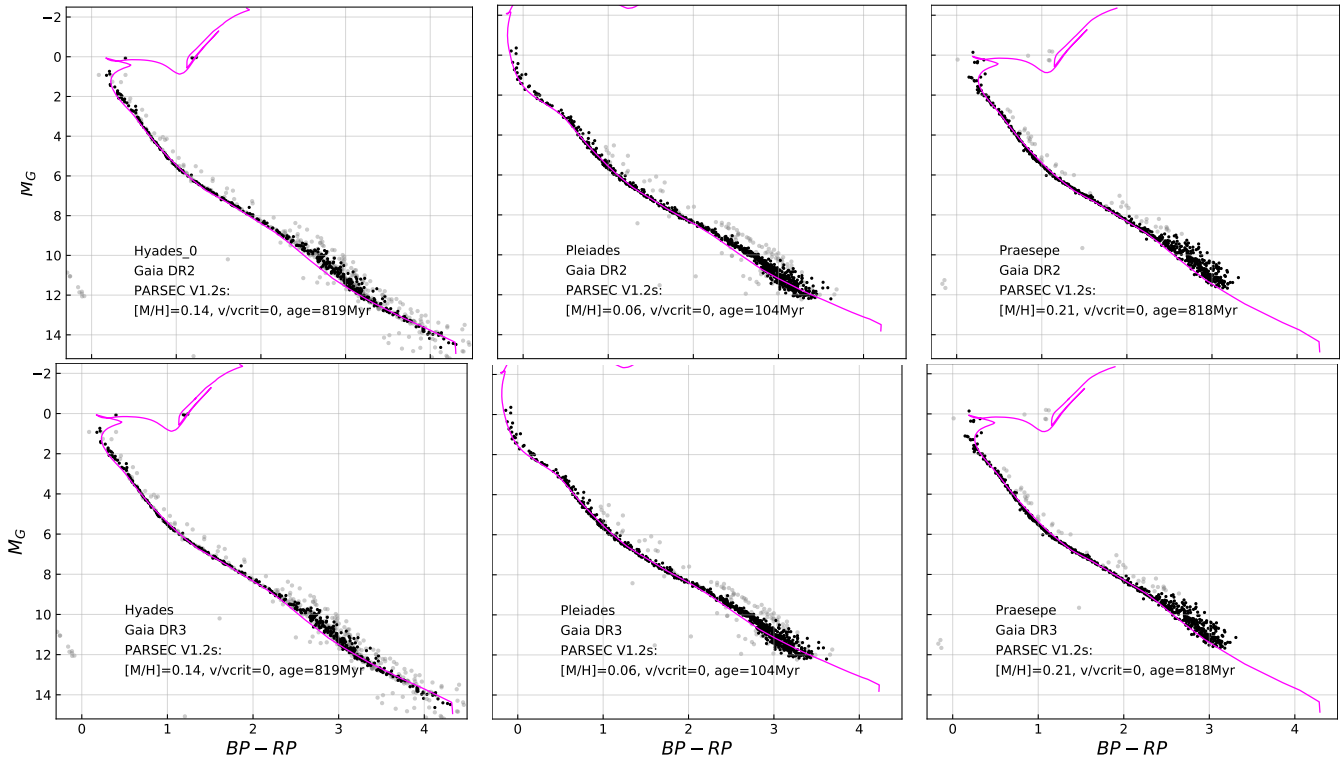


Figure 1. The CMDs of the clusters Hyades, Pleiades, and Praesepe (Upper panels: Gaia DR2; Lower panels: Gaia DR3). The magenta solid lines represent the isochrones from the PARSEC 1.2S model. Black dots represent cluster member stars obtained according to CG20 after removing potential field star contamination and binaries (described in section 3).

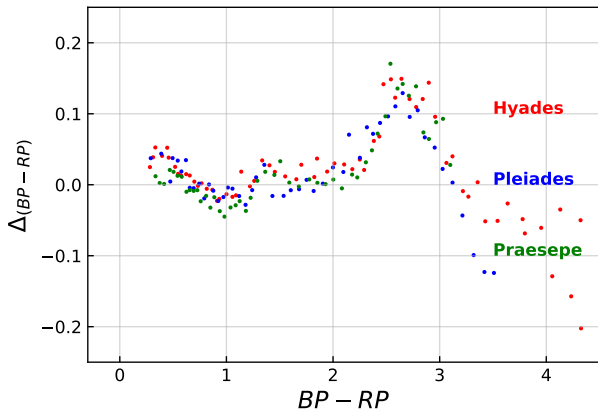


Figure 2. The distribution of the color deviation between the model isochrones and the Gaia DR3 data for the three clusters (red for Haydes, blue for Pleiades, and green for Praesepe).

CG20). Since CG20 membership is based on Gaia DR2, we cross-matched all their member stars with Gaia DR3 using a $1''$ radius. For each member star, we use the

code provided by the Gaia team² to correct the parallax zero point. We conducted 100,000 Gaussian distributed random samplings using the corrected-parallax and its error. Each sampled corrected-parallax was used to calculate distances through $\text{Distance/pc} = 1000/\text{parallax}$. We then computed the median and standard deviation of these 100,000 distance values, which were taken as the distance and its error of the star, respectively.

2.2. Isochrone models

Isochrones from two stellar evolutionary models are used in this work, they are both publicly available from their webpages. Here we introduce the settings we adopt to query the isochrones.

The MIST³ model, developed by the Modules for Experiments in Stellar Astrophysics (MESA, Paxton et al. 2011, 2013, 2015) project, encompasses stellar evolutionary tracks and isochrones. In this study, we utilize MIST isochrones without rotation, adopting solar-scaled abundance ratios with a metallicity of $Z_{\odot} = 0.0142$ (Asplund et al. 2009). These isochrones cover a wide range of ages ($5 \leq \lg(\tau/\text{yr}) \leq 10.3$), masses ($0.1 \leq M/M_{\odot} \leq 300$),

² https://gitlab.com/icc-ub/public/gaiadr3_zero_point

³ <http://waps.cfa.harvard.edu/MIST/index.html>

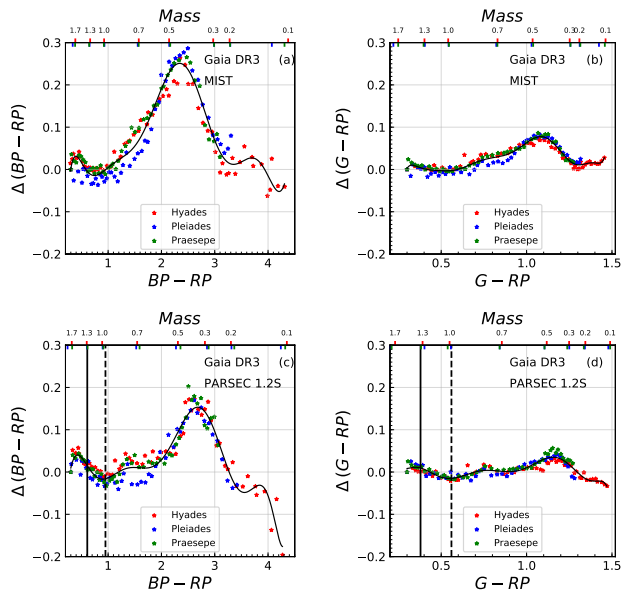


Figure 3. The distribution of the color deviation between the median color value in each color bin and that of the best fitted isochrones obtained from models MIST and PARSEC 1.2S. The color points correspond to the three benchmarked clusters. Color coding is identical to Figure 2. The solid black lines represent the trends of color deviations fitted using polynomial regression. Additionally, the colors corresponding to a temperature of approximately 5500 and 6500 K are indicated by the dashed and solid line in (c) and (d) panels, respectively.

and metallicities ($-2.0 \leq [Z/H] < 0.5$). The bolometric corrections used by MIST models are those derived from the PHOENIX models (Hauschildt et al. 1999a,b) (span the effective temperature $2000 K \leq T_{eff} \leq 10000 K$ and the gravity $-0.5 \leq \log(g) \leq 5.5$) and the COND model (Allard et al. 2001) (span the effective temperature $T_{eff} < 3000 K$).

The PARSEC (the PADova & TRIeste Stellar Evolution Code) isochrones used in this work are retrieved from the CMD web interface v3.7⁴. These isochrones are produced from PARSEC version 1.2S stellar tracks without rotation, which covers the metallicities $[M/H]$ range from -2.2 to 0.5 dex and the mass range from 0.1 to $350 M_{\odot}$. The corresponding bolometric corrections are produced with the default settings of YBC⁵ (Chen et al. 2019). Concerning the intermediate and low mass stars focused by this work, ATLAS9 spectral libraries (Castelli & Kurucz 2003) are used for the temperature range of $T_{eff} > 6500 K$, PHOENIX BT-Settl models (Allard et al. 2012) are used for cooler stars

with $T_{eff} < 5500 K$, a smooth interpolation of these two sets of atmosphere models are applied for stars with $6500 K > T_{eff} > 5500 K$).

In this work, the ranges of age and metallicity for the isochrones used are as follows: For both MIST and PARSEC models, we select isochrones with age ranging from $\lg(\tau/\text{yr}) = 6$ to 10 and a step of $\lg(\Delta\tau/\text{yr}) = 0.07$, as well as metallicity ($[Fe/H]$ or $[M/H]$) ranging from -0.05 to 0.25 dex. and a step of $\Delta[M/H]=0.05$ dex.

3. BENCHMARK CLUSTERS

As a well-defined single stellar population that formed in the same molecular cloud at the same time, open clusters have long been considered a good calibrator for stellar evolution and atmosphere models. The loci of an open cluster’s member stars on the CMD provide a laboratory for testing the agreement between theoretical predictions and observations.

We select Hyades, Pleiades, and Praesepe as our benchmark clusters to quantify the color deviation on CMD between Gaia DR3 observations and isochrone model predictions. These clusters are located relatively close to the Sun, with distances of approximately 40–50 pc, 130–140 pc, and 180–190 pc, respectively. They all show a clear single star sequence on CMD and are minimally affected by extinction (e.g., Bell et al. 2014; Kounkel & Covey 2019; Cantat-Gaudin et al. 2020). Previous literature provides age and metallicity estimates obtained through various calculation methods, as well as multi-band photometry and high-precision spectroscopic data. Table A.1 includes the ages and metallicities of the three clusters. According to the literature, the metallicity of the Hyades cluster ranges from 0 to 0.28 dex, with isochronal ages spanning from 500 Myr to 1 Gyr, and a Lithium Depletion Boundary (LDB) age of around 650 Myr. The Pleiades cluster exhibits a metallicity range of -0.039 to 0.1 dex, isochronal ages ranging from 50 to 141 Myr, and LDB ages ranging from 112 to 151 Myr. As for the Praesepe cluster, its metallicity falls between 0.08 and 0.27, with isochronal ages ranging from 600 to 794 Myr, and an LDB age of around 700 Myr.

Member stars of the three benchmark clusters are from the CG20 catalog as described in Sec 2.1. To obtain a single stellar sequence, we identify the main sequence ridge line of the cluster through number density and remove these stars with low photometric quality, where the color errors (σ_{BP-RP} and σ_{G-RP}) exceed 0.05 mag, and manually remove potential binaries, whose absolute magnitudes (M_G) differ from the main sequence ridge line by more than 0.4 mag, as well as field stars that are more than 0.4 mag below the ridge line. We also

⁴ <http://stev.oapd.inaf.it/cgi-bin/cmd>

⁵ <https://sec.center/YBC/>

remove the white dwarfs. Using this method, we removed 239(25%), 130(14%), and 62(9%) potential binaries, field stars and white dwarfs from the three clusters, respectively. We also performed de-reddening to cluster member stars. We utilized the three-dimensional extinction map SStructuring by Inversion the Local Interstellar Medium (STILISM⁶; Lallement et al. (2014); Capitanio et al. (2017); Lallement et al. (2018)) to calculate the color excess, $E(B-V)$, and its error, $\sigma_{E(B-V)}$, for each member in the clusters, and then determined the extinction $A_V = 3.1 \times E(B-V)$ and its propagated error σ_{A_V} . Next, by using the spectral data of main sequence stars from the Pickles library (Pickles 1998) and the extinction law proposed by Cardelli et al. (1989) (with $R_V = 3.1$), we obtain the extinction in bands (A_{BP} , A_{RP} , A_G) to calculate the de-reddened colors (BP–RP) and (G–RP), along with their errors $\sigma_{(BP-RP)}$ and $\sigma_{(G-RP)}$, and the de-reddened absolute magnitude M_G and its error σ_{M_G} . The extinctions from the clusters are independent on the colors and absolute magnitudes.

We calculate the median ages and metallicities provided in the references for the three clusters (see Table A.1), respectively. We then compare the CMDs of the clusters with the isochrones from the PARSEC 1.2S model, as depicted in Figure 1. From this figure, the discrepancy between the isochrones and the CMD of the clusters at the very low-mass part is evident. Such discrepancies have also been noted in Brandner et al. (2023a,b,c). The reason for the discrepancy is that the model either underestimates the observed stellar luminosity or predicts a bluer stellar color. For the former, Jeffries et al. (2017) proposed that for low-mass stars, magnetic field suppression of convection and the presence of numerous cool starspots could lead to stellar radius inflation, resulting in a systematic underestimation of stellar luminosity by the models. They further suggested that incorporating stellar radius inflation in the models could potentially reconcile the isochronal ages with the LDB ages. To address this issue, it may be necessary to reevaluate the stellar evolution models, a task that falls beyond the scope of this work. As for the latter, using empirical color corrections on the model isochrones may be a better approach. This approach allows the model isochrones to match the observations without including complicated physics, i.e., magnetic field and cool starspots in stellar evolution models discussing in Jeffries et al. (2017). In the CMDs (see Figure 1), we binned the M_G in intervals of 0.2 mag. For

each bin, we calculated the median color and its difference from the best fitted isochrones. Figure 2 shows that the color deviations for the three clusters exhibit a similar trend. Compared with the observations, the model PARSEC 1.2S colors are bluer for $2 \leq (BP-RP) \leq 3$ and redder for $(BP-RP) > 3$. Though the deviation generally small but much larger than the photometric uncertainties (0.002 mag, Gaia Collaboration et al. 2023). Therefore, empirically correcting the colors can improve the fit between the model isochrones and the CMDs of the clusters.

4. EMPIRICAL COLOR CORRECTIONS

In this section, we demonstrate how to perform empirical color (BP–RP and G–RP) corrections on the MIST and PARSEC 1.2S models using the three benchmark clusters.

In previous works, the M_G versus (BP–RP) CMD is widely used to fit model isochrones (see e.g., Cantat-Gaudin et al. 2020; Kounkel & Covey 2019; Dias et al. 2021; Hunt & Reffert 2024). However, the Gaia BP band is slightly less reliable compared to the other two bands. As discussed in the Gaia DR2 photometry validation paper (Evans et al. 2018), the Gaia BP magnitude band show a larger calibration uncertainty with respect to RP and G magnitude bands. From the Early DR3 of Gaia, the overall photometry uncertainty for the three passbands is improved to an even better level compared to the previous data releases, but the BP band is still more affected by calibration issues and is the less good one among the three bands. In this study, we work on CMD based on the widely used colors (BP–RP) and (G–RP).

We use the model isochrones to fit CMDs of the benchmark clusters. To avoid possible fitting uncertainties introduced by the color deviations on the low-mass part as described before, we select the blue and bright members for the CMD fittings. As shown in Figures 2 or 3(c), the color deviations between the PARSEC 1.2S isochrones and the cluster are relatively small within the range of $(BP-RP) \leq 2$ mag. Similarly, as shown in Figure 3(d), the color deviations are small within the range of $(G-RP) \leq 1$ mag. To maintain consistency in the color correction range, we selected cluster members within the color ranges of $(BP-RP) \leq 2$ mag and $(G-RP) \leq 1$ mag for the first iteration and fitted them with the PARSEC 1.2S and MIST models to obtain the best-fitted isochrones. Although, as shown in Figures 3(a) and (b), the MIST model exhibits noticeable deviations in these color ranges, the effects from these deviations are effectively mitigated after multiple iterations. Using the method as described in Liu & Pang (2019), for each cluster member, we calculate the small-

⁶ <https://stilism.obspm.fr>

est departure to a model isochrone, and compute the mean departure of all members to that isochrone. Note that we don't apply any weighting during the fitting. The isochrone with the shortest mean departure is taken as the best-fit one, and its age is considered as the age of the cluster. On the CMD, we bin the M_G in intervals of 0.2 mag. For each bin, we calculate the median color and its difference between the cluster members and the best-fitting isochrones. The overall trend of these color differences is consistent for the three clusters. We use the polynomial fitting method to fit the color differences of the clusters and obtain an initial color correction function.

Next, we apply the initial color correction function obtained above to the model isochrones and use isochrones with corrected color to refit the CMDs of the clusters. The initial color correction function reduces the color deviations between the model isochrones and the benchmark clusters. Therefore, the range of colors (BP–RP) and (G–RP) used in this fitting process includes the entire color range of the clusters. We recalculate the mean distances between the color-corrected model isochrones and the cluster members and determine the best-fitting isochrone by the shortest mean distance. We then bin the M_G with a 0.2 mag interval in the CMD. For each bin, we calculate the median color and its difference between the clusters and the best-fitting isochrones. In Figure 3, we show the color differences between the three clusters and the best-fitting isochrones from the MIST and PARSEC 1.2S models, respectively. In these four subplots, we observe that the trends of the color differences are generally consistent. We then use the polynomial fitting method to refit the differences and obtain an empirical color correction function for the differences. We represent the color-corrected function with black solid lines in Figure 3. The color-correction function obtained the color deviation (f) between the model isochrone and the observation is given as follows:

$$f(x) = \sum_{i=0}^N k_i x^{N-i}, \quad (1)$$

where x represents the color (BP–RP) or (G–RP). The values of the coefficients k_i and the polynomial degree N for MIST and PARSEC 1.2S models are all listed in Table 1. When fitting the overall trend of color deviation, we determine the best-fitted value of N by comparing the goodness of fit between the original data and the fitted curve data, choosing the smallest integer where the goodness of fit exceeds 98%.

To correct the model isochrones, we calculate the color correction functions and add them to the model isochrone colors. In Figures 4 and 5, as well as Fig-

ures B.1 to B.2, we display the comparison of the best-fitting isochrones for the three clusters in CMDs before and after color correction. The uncertainty in age is obtained by performing bootstrap resampling on the colors (BP–RP and G–RP) and the absolute magnitude (M_G), selecting only 50% of the data in each sample. This process is repeated 1000 times, and the 68% quantile of the results is calculated. We summarize these results in Table 2.

5. APPLICATION TO OTHER STELLAR SYSTEMS

To check whether the color deviation of the original isochrones affects age determinations, in this section we apply the empirical color correction functions obtained in Section 4 to fit CMDs of other star clusters and moving groups. We then compare and discuss these results with isochronal ages and LDB ages provided in the literature.

5.1. Application for color correction

We selected 31 open clusters from CG20 with low extinction A_V , located at relatively short distances (approximately less than 1 kpc), and with a substantial number of member stars (more than 150). Additionally, we chose three young moving groups, namely β Pictoris (BPMG), 32 Ori (THOR) (Gagné et al. 2018), and Tucana-Horologium moving group (THMG) (Galli et al. 2023), which are also nearby (within 200 pc). The ages and metallicities of these 31 clusters and 3 moving groups were obtained from these literature, where the ages were derived either from isochrone fitting across multiple photometric bands or from LDB, and the metallicities were either derived from isochrone fitting or from spectroscopic data. According to the literature, the ages of these clusters and moving groups range from a few million years to over 1 Gyr, with metallicities spanning from -0.1 to 0.15 .

We cross-matched the CG20 catalog members of these 31 clusters and 3 moving groups with Gaia DR3 within a radius of $1''$ and applied reddening correction. We obtained the dereddened colors (BP–RP) and (G–RP), along with their errors $\sigma_{(\text{BP-RP})}$ and $\sigma_{(\text{G-RP})}$, as well as the dereddened absolute magnitude M_G and its error σ_{M_G} for each member. Following the method outlined in Section 3, we used the empirically color-corrected isochrones obtained from Section 4 to fit the CMDs of these clusters and moving groups and calculated the mean distances between the model isochrones and the members, and then determine the best-fitting isochrone by the shortest mean distance. For each star cluster and moving group, we perform same method described in Section 4 to calculate age and its uncertainty.

Table 1. The coefficients for the color correction functions in Section 4.

	MIST		PARSEC 1.2S	
	BP-RP	G-RP	BP-RP	G-RP
k_0	-4.84109156662e-03	1.66041686674e+03	4.43946646259e-03	-1.55281212469e+02
k_1	1.18790335297e-01	-1.56566075272e+04	-8.99126898611e-02	1.19242974533e+03
k_2	-1.24788718579e+00	6.55134171293e+04	7.57462148449e-01	-3.93129271756e+03
k_3	7.34202485899e+00	-1.60375747677e+05	-3.41507655298e+00	7.27822027924e+03
k_4	-2.65953606912e+01	2.54904982070e+05	8.75609327100e+00	-8.30782701688e+03
k_5	6.14897637911e+01	-2.75935718076e+05	-1.21266013380e+01	6.03969724150e+03
k_6	-9.11778295307e+01	2.07427644403e+05	6.13317544359e+00	-2.78554182219e+03
k_7	8.49214572624e+01	-1.08227497419e+05	5.20844674997e+00	7.83342648627e+02
k_8	-4.69874927204e+01	3.84024814235e+04	-8.76070696284e+00	-1.21713434987e+02
k_9	1.37158168882e+01	-8.82591877952e+03	4.12464395718e+00	7.97636109336e+00
k_{10}	-1.56992702563e+00	1.18259672423e+03	-6.05928788398e-01	0
k_{11}	0	-6.99859722054e+01	0	0

Column 1: the coefficients of the color correction functions. Column 2–3: the coefficients of the color correction functions for the (BP-RP) and (G-RP) colors, respectively, based on the MIST model. Column 4–5 the coefficients of the color correction functions for the (BP-RP) and (G-RP) colors, respectively, based on the PARSEC 1.2S model.

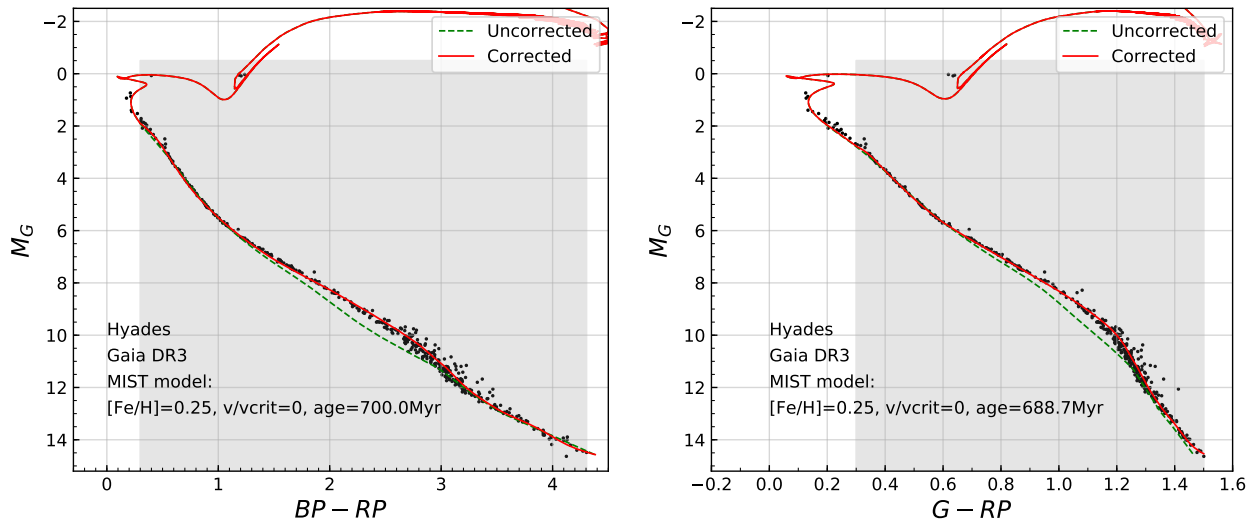


Figure 4. CMDs of Hyades open cluster used by MIST model. The data are from Gaia DR3 (Gaia Collaboration et al. 2023). The member candidates are manually selected because of the existence of likely binary or multiple stars and white dwarf stars, in short, most of them are bonafide single stars (according to the work provided by Brandner et al. (2023c)).

In Figures 6 and others in Appendix C, we show the isochrones before and after color correction with the distributions of stars in the clusters and associations in CMDs. From these figures, we can see that the isochrones after the empirical color correction align significantly better with the observational CMDs of the clusters and moving groups. Only a few clusters exhibit less noticeable contrasts due to the lack of member stars in the low-mass regime. The ages and metallicities recomputed in this study for the clusters and associations are summarized in Table 3.

We derive the cluster ages from isochrones without corrections using the method described in Section 4, and compare them with the ones obtained with the corrections in Figure 7. The ages obtained without correction are generally younger. This is especially evident for the clusters with the low-mass stars ($\leq 0.6 M_{\odot}$). As shown in Figure 2, When $(BP-RP) \geq 2$ mag, the isochrones tend to be bluer than the observations. Due to this effect, the isochrone fits including the low-mass stars result in the younger ages by 0.075 dex in $\log(\text{age})$ than the ones from the corrected isochrone. For the clusters without

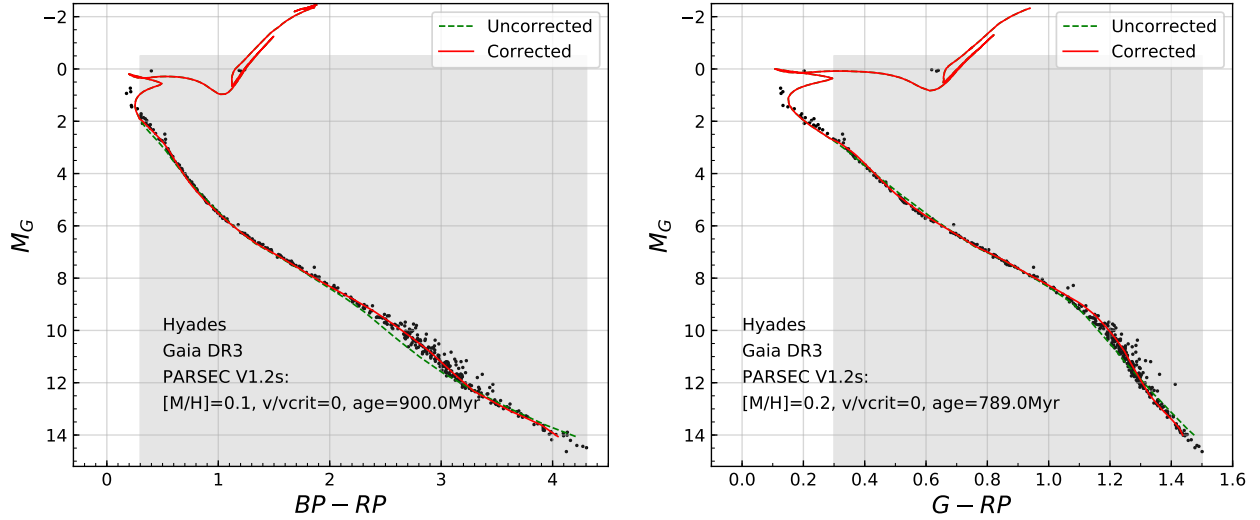


Figure 5. CMDs of Hyades open cluster used by PARSEC model. Similar to Figure 4.

Table 2. Ages and metallicities of the Hyades, Pleiades and Praesepe open clusters calculated from the perspective of M_G versus (BP-RP) and (G-RP) based on the MIST and PARSEC 1.2S isochrone models.

Cluster	MIST				PARSEC 1.2S			
	BP-RP		G-RP		BP-RP		G-RP	
	[Fe/H]	Age/Myr	[Fe/H]	Age/Myr	[M/H]	Age/Myr	[M/H]	Age/Myr
Hyades	0.25 ± 0.0	700^{+75}_{-142}	0.25 ± 0.0	688.7 ± 100	$0.10^{+0.05}_{-0.0}$	900^{+15}_{-162}	0.20 ± 0.05	789^{+98}_{-62}
Pleiades	0.25 ± 0.0	206^{+16}_{-66}	0.25 ± 0.0	202.7^{+13}_{-65}	$0.10^{+0.0}_{-0.05}$	152 ± 27	$0.10^{+0.0}_{+0.05}$	133 ± 13
Praesepe	0.25 ± 0.05	656^{+116}_{-90}	0.25 ± 0.0	666.7	0.15 ± 0.0	738^{+47}_{-91}	0.15 ± 0.05	776^{+73}_{-107}

Column 1: the names of the open clusters. Columns 2-3: Best-fit age and metallicity obtained by fitting isochrones from the MIST model with (BP-RP) isochrone colors. Columns 4-5: Best-fit age and metallicity obtained by fitting isochrones from the MIST model with (G-RP) isochrone colors. Columns 6-7: Best-fit age and metallicity obtained by fitting isochrones from the PARSEC 1.2S model with (BP-RP) isochrone colors. Columns 7-8: Best-fit age and metallicity obtained by fitting isochrones from the PARSEC 1.2S model with (G-RP) isochrone colors.

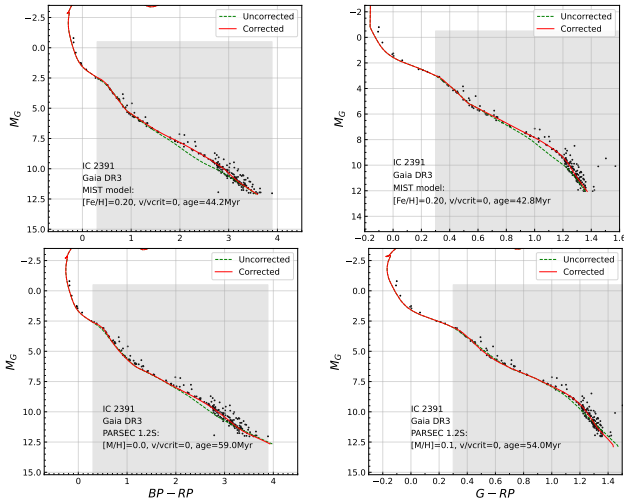


Figure 6. CMDs of IC 2391.

the low-mass stars, the two sets of ages agree with each other within 0.01 dex.

It worth noting that the age determination, no matter which method is applied, is highly sensitive to the quality of data and the physics detail of models. The isochrone fitting method on CMDs is particularly good with non-negligible uncertainties, especially for young stellar populations with $\lesssim 50$ Myr. For stars with this young age, it is very challenging to model their magnetic field, as well as the bolometric corrections with starspots and accretion disc, which affect the stellar color and brightness. Therefore, in this work we can only provide a rough estimate of the age parameter and use it to assess the formation and evolutionary status of star clusters or moving groups with very young age.

5.2. Comparison with Ages from Other Literature

In this subsection, we compare the ages and metallicities of the clusters and associations obtained from this work with those provided in the literature (see Table C.1).

Table 3. Ages and metallicities of the 31 clusters and 3 moving groups calculated from the perspective of M_G versus (BP–RP) and (G–RP) based on the MIST and PARSEC 1.2S isochrone models.

Cluster	MIST				PARSEC 1.2S			
	BP–RP		G–RP		BP–RP		G–RP	
	[Fe/H]	Age/Myr	[Fe/H]	Age/Myr	[M/H]	Age/Myr	[M/H]	Age/Myr
NGC 752	$0.10^{+0.05}_{-0.0}$	1176^{+163}_{-19}	0.10 ± 0.10	1235^{+529}_{-83}	$-0.05^{+0.1}_{-0.05}$	1382^{+110}_{-151}	$-0.05^{+0.1}_{-0.05}$	1405^{+359}_{-378}
NGC 7092	0.10 ± 0.0	332^{+120}_{-11}	0.10 ± 0.10	297^{+141}_{-94}	$0.00^{+0.05}_{-0.05}$	335^{+46}_{-69}	$0.00^{+0.0}_{-0.05}$	340^{+118}_{-6}
NGC 2516	0.25 ± 0.05	656^{+58}_{-86}	0.25 ± 0.05	667 ± 28	0.15 ± 0.05	738^{+24}_{-52}	$0.15^{+0.05}_{-0.0}$	776^{+105}_{-46}
Blanco 1	0.15 ± 0.05	101^{+17}_{-21}	0.15 ± 0.10	99 ± 32	$0.00^{+0.05}_{-0.00}$	135^{+14}_{-15}	$0.00^{+0.05}_{-0.0}$	117^{+19}_{-7}
NGC 2451B	$0.25^{+0.0}_{-0.05}$	38^{+4}_{-1}	0.20 ± 0.05	36 ± 12	$0.00^{+0.1}_{-0.05}$	41^{+9}_{-7}	$0.00^{+0.1}_{-0.05}$	33^{+5}_{-3}
IC 2602	$0.25^{+0.0}_{-0.05}$	40^{+8}_{-1}	0.25 ± 0.05	43 ± 14	$0.10^{+0.1}_{-0.05}$	59^{+8}_{-1}	0.20 ± 0.05	61^{+1}_{-6}
IC 2391	0.20 ± 0.05	44^{+8}_{-1}	0.20 ± 0.05	43 ± 14	$0.00^{+0.15}_{-0.05}$	59^{+11}_{-3}	0.10 ± 0.05	54^{+4}_{-9}
NGC 2232	$0.15^{+0.10}_{-0.0}$	27^{+4}_{-1}	0.15 ± 0.10	26 ± 9	-0.05 ± 0.05	32^{+1}_{-2}	-0.05 ± 0.05	28^{+1}_{-3}
Pozzo 1	$0.25^{+0.0}_{-0.05}$	16 ± 1	0.25 ± 0.05	15 ± 5	$-0.05^{+0.0}_{-0.1}$	14 ± 1	-0.05 ± 0.05	12 ± 1
Alessi 3	$0.10^{+0.05}_{-0.0}$	760^{+12}_{-228}	0.1 ± 0.10	615^{+249}_{-222}	$0.00^{+0.0}_{-0.05}$	738^{+77}_{-70}	$0.00^{+0.1}_{-0.0}$	703^{+73}_{-189}
ASCC 101	0.15 ± 0.05	397^{+20}_{-70}	0.20 ± 0.05	366^{+165}_{-72}	$0.00^{+0.05}_{-0.0}$	450^{+61}_{-127}	0.05 ± 0.05	450^{+72}_{-68}
Alessi 9	0.15 ± 0.05	283^{+5}_{-67}	0.20 ± 0.05	372^{+177}_{-66}	0.00 ± 0.05	340^{+132}_{-17}	$0.10^{+0.0}_{-0.05}$	382^{+141}_{-48}
ASCC 41	0.15 ± 0.05	227^{+11}_{-24}	0.15 ± 0.10	227 ± 85	$0.00^{+0.0}_{-0.05}$	218^{+48}_{-71}	$0.00^{+0.05}_{-0.0}$	357^{+57}_{-100}
NGC 2422	$0.25^{+0.0}_{-0.05}$	104^{+1}_{-14}	0.25 ± 0.05	104 ± 34	0.10 ± 0.05	125^{+04}_{-10}	$0.15^{+0.0}_{-0.05}$	165^{+5}_{-50}
Teutsch 35	$0.25^{+0.0}_{-0.05}$	113^{+36}_{-30}	0.25 ± 0.05	200^{+2}_{-3}	$0.10^{+0.05}_{-0.0}$	127^{+58}_{-10}	$0.15^{+0.05}_{-0.0}$	222^{+108}_{-15}
UPK 612	$0.20^{+0.05}_{-0.0}$	113^{+14}_{-22}	0.25 ± 0.05	142^{+54}_{-46}	$0.00^{+0.05}_{-0.05}$	123^{+28}_{-11}	$0.10^{+0.05}_{-0.0}$	176^{+73}_{-32}
Roslund 6	0.15 ± 0.05	99^{+2}_{-20}	0.20 ± 0.05	187^{+13}_{-9}	$-0.05^{+0.05}_{-0.05}$	106^{+36}_{-17}	$0.05^{+0.05}_{-0.0}$	157^{+72}_{-19}
Platais 9	$0.20^{+0.05}_{-0.0}$	59^{+2}_{-6}	0.25 ± 0.05	65 ± 21	$0.05^{+0.05}_{-0.0}$	75^{+5}_{-7}	$0.10^{+0.05}_{-0.0}$	71^{+5}_{-6}
NGC 2451A	$0.20^{+0.05}_{-0.0}$	$52^{+2}_{-30.1}$	0.20 ± 0.05	49 ± 16	$0.00^{+0.05}_{-0.0}$	62^{+4}_{-3}	$0.05^{+0.10}_{-0.0}$	59 ± 5
RSG 5	0.25 ± 0.0	49^{+1}_{-2}	0.25 ± 0.05	49 ± 16	$0.00^{+0.1}_{-0.0}$	49^{+9}_{-2}	0.10 ± 0.05	53^{+4}_{-7}
Trumpler 10	0.25 ± 0.0	52 ± 1	0.25 ± 0.05	51 ± 16	$0.10^{+0.05}_{-0.0}$	62^{+2}_{-3}	$0.15^{+0.0}_{-0.05}$	62^{+2}_{-7}
NGC 2547	$0.25^{+0.0}_{-0.05}$	42^{+1}_{-5}	0.20 ± 0.05	36 ± 12	$-0.05^{+0.05}_{-0.0}$	37 ± 3	$0.00^{+0.10}_{-0.0}$	35^{+5}_{-2}
BH 164	$0.25^{+0.05}_{-0.0}$	42^{+1}_{-5}	0.25 ± 0.05	37 ± 12	$0.00^{+0.1}_{-0.0}$	40^{+7}_{-2}	$0.10^{+0.1}_{-0.0}$	40^{+8}_{-3}
NGC 3228	0.20 ± 0.05	34^{+3}_{-2}	0.25 ± 0.05	36 ± 12	$0.05^{+0.1}_{-0.05}$	36 ± 6	$0.15^{+0.0}_{-0.05}$	33 ± 3
Col 140	$0.25^{+0.0}_{-0.05}$	42^{+1}_{-4}	0.20 ± 0.05	38 ± 12	$-0.05^{+0.15}_{-0.0}$	37^{+13}_{-3}	$-0.05^{+0.15}_{-0.0}$	35^{+14}_{-3}
Col 135	$0.25^{+0.0}_{-0.05}$	44^{+1}_{-5}	0.20 ± 0.05	38 ± 12	$0.00^{+0.1}_{-0.0}$	44^{+6}_{-4}	$0.10^{+0.05}_{-0.0}$	47^{+6}_{-5}
UBC 17b	0.15 ± 0.05	10 ± 3	0.25 ± 0.05	12 ± 4	$-0.05^{+0.05}_{-0.0}$	10^{+1}_{-2}	$0.10^{+0.10}_{-0.15}$	9^{+3}_{-2}
ASCC 21	$0.25^{+0.0}_{-0.1}$	14^{+1}_{-3}	0.25 ± 0.05	13 ± 4	-0.05 ± 0.0	12 ± 1	0.00 ± 0.05	13^{+1}_{-4}
NGC 2281	$0.20^{+0.05}_{-0.0}$	490^{+87}_{-158}	0.20 ± 0.05	423^{+191}_{-108}	$0.00^{+0.05}_{-0.0}$	637^{+43}_{-155}	$0.05^{+0.0}_{-0.05}$	616^{+67}_{-135}
NGC 1960	$0.20^{+0.05}_{-0.1}$	21^{+1}_{-2}	0.20 ± 0.05	21 ± 7	$0.15^{+0.0}_{-0.05}$	21^{+1}_{-2}	0.15 ± 0.10	21^{+1}_{-4}
IC 4665	0.25 ± 0.0	41^{+2}_{-5}	0.25 ± 0.05	38 ± 13	$0.15^{+0.1}_{-0.05}$	47^{+11}_{-7}	$0.25^{+0.0}_{-0.05}$	48^{+2}_{-9}
BPMG	0.10 ± 0.05	21 ± 3	$0.25^{+0.0}_{-0.05}$	25 ± 5	$-0.05^{+0.10}_{-0.0}$	23^{+2}_{-3}	$-0.05^{+0.05}_{-0.0}$	19 ± 3
THOR	$0.25^{+0.0}_{-0.05}$	22 ± 4	$0.25^{+0.0}_{-0.05}$	19^{+1}_{-3}	$-0.05^{+0.05}_{-0.0}$	20 ± 3	$-0.05^{+0.05}_{-0.0}$	15^{+4}_{-3}
THMG	$0.25^{+0.0}_{-0.05}$	48^{+1}_{-5}	$0.25^{+0.0}_{-0.05}$	50 ± 5	0.15 ± 0.05	55^{+2}_{-6}	$0.15^{+0.05}_{-0.0}$	55 ± 5

Column 1: the names of the open clusters. Columns 2-3: Best-fit age and metallicity obtained by fitting isochrones from the MIST model with (BP–RP) isochrone colors. Columns 4-5: Best-fit age and metallicity obtained by fitting isochrones from the MIST model with (G–RP) isochrone colors. Columns 6-7: Best-fit age and metallicity obtained by fitting isochrones from the PARSEC 1.2S model with (BP–RP) isochrone colors. Columns 7-8: Best-fit age and metallicity obtained by fitting isochrones from the PARSEC 1.2S model with (G–RP) isochrone colors.

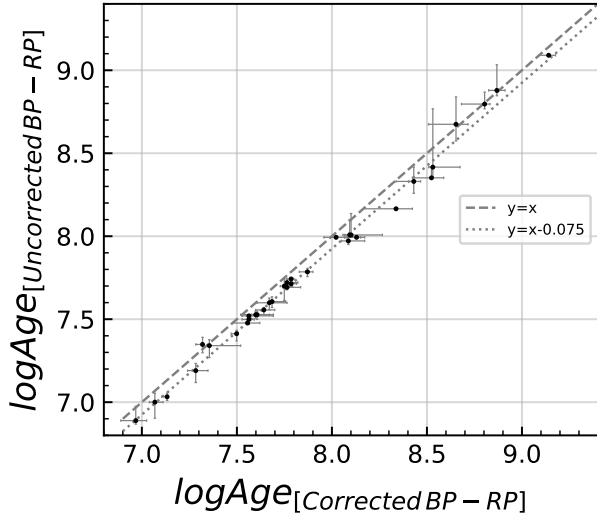


Figure 7. Comparison between the ages derived from the corrected color (BP–RP) model PARSEC 1.2S isochrones and the original color model isochrones for 31 star clusters and 3 moving groups. The dashed line represents a 1:1 ratio, while the dot-dashed lines are offset by 0.075 dex from the dashed line.

In Figure 8, we compare the ages from the MIST and PARSEC 1.2S isochrones. The ages and their uncertainties for each model are the mean and the dispersion of the isochronal ages from the two CMDs (see Section 5.1), G vs. $(G-RP)$ and G vs. $(BP-RP)$. From this figure, we observe that for clusters and associations with $\log \text{Age} \geq 7.5$, the PARSEC isochronal ages tend to be slightly older, while for those with $\log \text{Age} \leq 7.5$, they appear slightly younger. However, almost all clusters and associations exhibit isochronal age distributions that fall within their respective 1σ error ranges.

In addition to comparing ages, we also assessed the differences in metallicity obtained from the empirical color corrections applied to the two models in Figure 9. Based on the metallicities provided by spectroscopic data for each cluster and moving group (see Table C.1) and those obtained from fitting with the empirically color-corrected MIST and PARSEC 1.2S models, we calculated the median values and their differences, yielding values of 0.21 ± 0.10 dex and 0.03 ± 0.13 dex, respectively. From the distribution in this figure, it can be observed that when fitting for the best ages and metallicities using the empirically color-corrected MIST and PARSEC 1.2S models separately, the metallicities derived from the MIST model tend to be slightly more enriched, while those from the PARSEC 1.2S model are closer to the spectroscopic metallicities. We also obtained the ages and metallicities of the clusters from fitting their CMDs with $M_G < 8$ (i.e., excluding low-mass stars), and com-

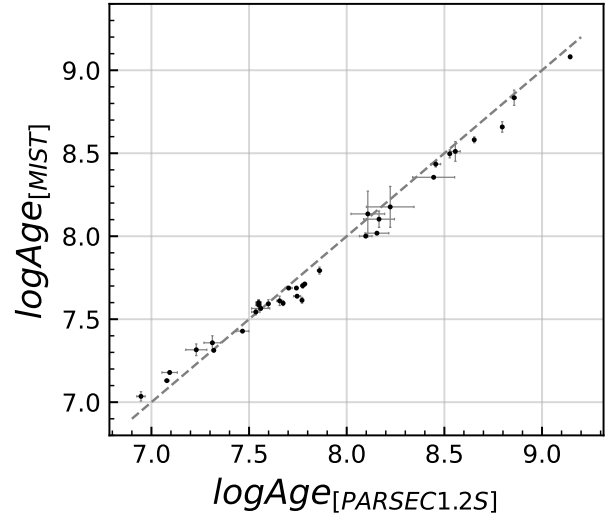


Figure 8. Comparison between the ages obtained from the PARSEC 1.2S model and those obtained from the MIST model for the 31 clusters and 3 moving groups in this work. The grey dashed line represents the ratio 1:1, as in Figure 7.

pared these metallicities with those from spectroscopic data. The median differences and standard deviations are 0.21 ± 0.10 dex and 0.04 ± 0.14 dex, respectively, which are consistent with the results in the above (including low-mass stars).

As shown in the left panel of Figure 10, we compare the ages of clusters and moving groups calculated using the PARSEC 1.2 model in this work (see Section 5.1) with those provided in the literature by taking their median and error values. In this subplot, we observe that the age distributions of almost all clusters and moving groups are consistent within the 1σ error range. In the right panel, we further compare the ages of clusters calculated using the PARSEC 1.2 model in this work, considering their median and error values, with those provided by CG20. From the plot, it is evident that for clusters with $\log \text{Age} \geq 8$, which are relatively older, the age distributions are nearly identical within the 1σ error range. However, for clusters with $\log \text{Age} \leq 8$, which are relatively younger, CG20’s isochronal ages tend to be younger. This suggests that the ages recalculated after empirical color corrections tend to be slightly older. This difference may arise because CG20’s age calculations involve fitting the entire CMD of the cluster, including the very low-mass part with color deviations. Whilst our empirical color corrections to the very low-mass part of the isochrones have a better agreement to the observations with a slightly redder color.

The Lithium Depletion Boundary (LDB) method is an independent method comparing with other model-dependant techniques, such as isochrone fitting, for de-

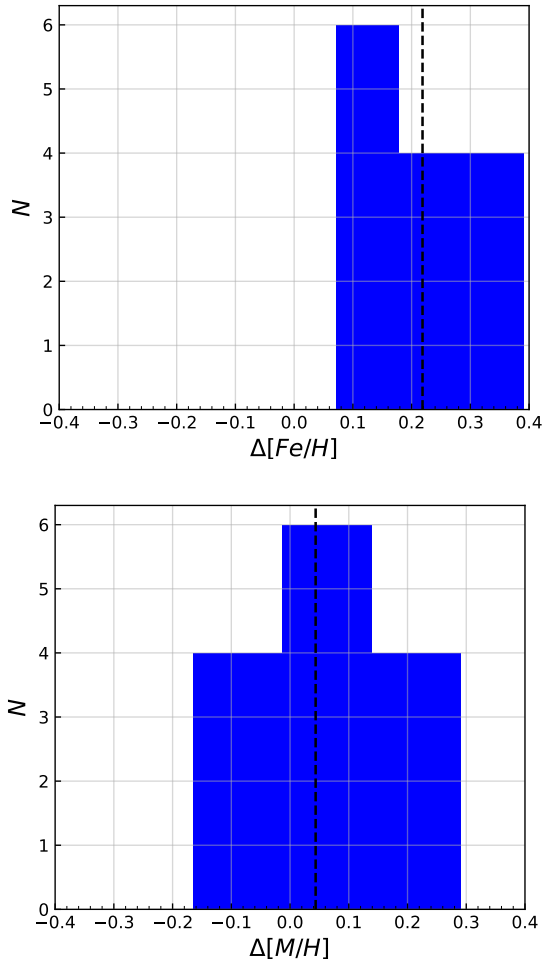


Figure 9. The distribution of differences between the metallicities obtained for the 31 clusters and 3 moving groups in this work and those obtained from spectroscopic data in the literature. The upper panel illustrates the difference distribution between the metallicities obtained from the MIST model in this work and those derived from spectroscopic data in the literature. The lower panel shows the difference distribution between the metallicities obtained from the PARSEC 1.2S model in this work and those derived from spectroscopic data in the literature. The black solid line represents the median difference.

terminating the ages of stellar groups and is based on measuring the strength of the lithium line in low-mass stars and brown dwarfs (Basri et al. 1996; Rebolo et al. 1996; Burke et al. 2004). In the low mass range, the lithium burning process is very rapid and highly dependent on mass, leading to a distinct boundary between lithium-rich and lithium-poor cluster members (e.g., D’Antona & Mazzitelli 1994; Bildsten et al. 1997). By identifying the brightest lithium-rich star as the upper boundary and the faintest lithium-poor star as the lower boundary, and comparing these with theoretical

models, the cluster’s age can be determined. As shown in Figure 11, to compare the LDB ages provided in the literature with the ages obtained in this work after empirical color correction using the PARSEC 1.2S model, we calculated the median and standard deviation of the LDB ages for the 8 open clusters and 3 moving groups listed in Table C.1, respectively. From the distribution in this plot, it can be seen that the ages of the vast majority of clusters and moving groups are nearly identical. Although there are a few clusters and groups whose ages obtained in this study slightly differ from the LDB ages, such as NGC 2232 and THMG, they still fall within the 3σ range of LDB age errors.

6. SUMMARY AND DISCUSSIONS

In this work, we quantify the color deviations between Gaia DR3 CMD of open clusters and model isochrones, focusing on the low-mass part (approximately $M \approx 0.3 \sim 0.6 M_{\odot}$). Using the empirical color corrections on (BP–RP) and (G–RP) to the currently available MIST and PARSEC 1.2S isochrones, we re-determine the age of 31 open clusters and 3 moving groups.

Three nearby open clusters with low extinction and well-constrained age serve as the benchmark clusters in this study: Hyades, Pleiades, and Praesepe. We quantify the color discrepancies between these benchmark clusters and their best-fitted isochrones. Subsequently, we derive empirical color correction functions via polynomial fitting, particularly at low masses. The (BP–RP) color correction has a maximum value of ~ 0.25 mag for MIST and ~ 0.15 mag for PARSEC 1.2S. The (G–RP) color correction is slightly smaller, with a maximum value of ~ 0.08 mag for MIST and ~ 0.04 mag for PARSEC 1.2S.

Based on the isochrones with empirical color correction functions, we recalculate the age of these open clusters and moving groups. The recalculated ages are consistent with the literature values based on the spectral LDB method within the 3σ error range. Additionally, the ages obtained from original isochrones are younger by ~ 0.075 dex in log Age compared to those from empirically color-corrected isochrones. However, it’s important to acknowledge that isochrone fitting for very young stellar populations carries larger uncertainties compared to older stars. For the very young clusters and moving groups we can only offer a rough age estimate using the homogeneous age determination method.

The empirical color corrections we present in this work, can serve the community as a tool for reliable age determination using the current available isochrone models. However, the underlying cause of the model-observation color discrepancies in this

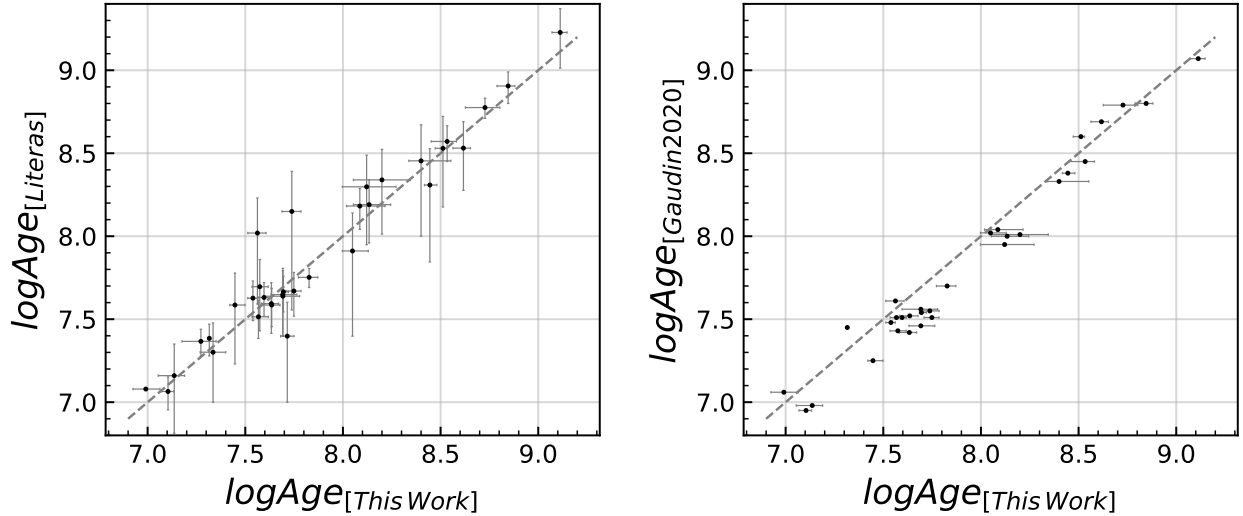


Figure 10. Comparison of the ages obtained from the PARSEC model for the 31 clusters and 3 moving groups in this work with those in the literature. Left panel: Comparison with ages from the literature. Right panel: Comparison with ages provided by CG20. The grey dashed line represents the ratio 1:1, the same as in the preceding Figure 7 and 8.

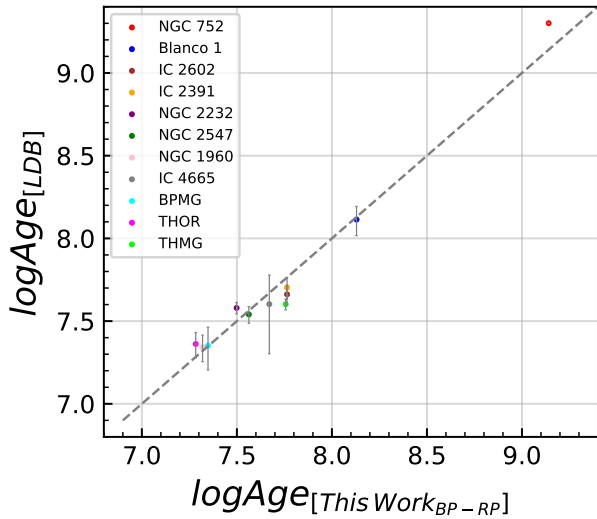


Figure 11. Comparison of ages for 8 star clusters and 3 moving groups. Ages derived from the best-fitting isochrones using color ($BP-RP$) and its color-corrected version are compared with the LDB ages. The grey dashed line represents the ratio 1:1, the same as in the preceding Figures 7, 8, and 10.

mass/color/temperature regime remains elusive. Here we list several possible factors that may contribute to the observed color discrepancy.

- Limited understanding of the Gaia photometry: With Gaia being the sole source for such high-precision photometry data for a large number of low-mass stars in open clusters, the color discrepancy may have gone unnoticed previously. Additionally, the possibility of unknown issues with

Gaia passband bolometric corrections or photometry itself cannot be entirely ruled out.

- Stellar rotation: Rotational speed and inclination angle can influence stellar color (see e.g. Costa et al. 2019; Nguyen et al. 2022; Girardi et al. 2019). While rotation has minimal impact on the structure of the low-mass stars we focus on (being fully convective, see discussions in Bressan et al. (2012); Fu et al. (2015), and geometrical distortion discussed in Girardi et al. (2019)), the inclination angle can affect their bolometric correction. As shown by Girardi et al. (2019), fast rotation stars appear redder when viewed from the equator compared to the pole.
- Magnetic fields: As mentioned earlier for young stellar populations, magnetic fields can also affect stellar color. However, constraining and modeling magnetic fields remains a significant challenge observationally and theoretically.

Future research efforts focus on a deeper understanding of these potential contributors may help to unfold the hidden nature of the color discrepancy we discussed in this work.

It is worth noting that in this work we choose to use the trigonometric parallax method to calculate the distances of star cluster and moving group members. This method has a distance error of approximately 1 pc within a range of 500 pc, which is relatively small and can be neglected. However, the method is not suitable to the distant cluster members because of the larger distance errors.

This work is supported by the National Key Research and Development Program of China (2023YFA1608100). X.F. thanks the support of the National Natural Science Foundation of China (NSFC) No. 12203100 and the China Manned Space Project with No. CMS-CSST-2021-A08. Y.C. acknowledges National Natural Science Foundation of China (NSFC) No. 12003001. Xiaoying Pang acknowledges the financial support of the National Natural Science Foundation of China through grants 12173029 and 12233013. L.Li thanks the support of NSFC No. 12303026 and the Young Data Scientist Project of the National Astronomical Data Center. W.Cui thanks the support of NSFC No. 12173013.

Z. Li thanks the support of NSFC No. 12473029. This work has made use of data from the European Space Agency (ESA) mission Gaia (<http://www.cosmos.esa.int/gaia>), processed by the Gaia Data Processing and Analysis Consortium (DPAC, <http://www.cosmos.esa.int/web/gaia/dpac/consortium>). This research has made use of the TOPCAT catalogue handling and plotting tool (Taylor 2005); of the Simbad database and the VizieR catalogue access tool, CDS, Strasbourg, France; and of NASA's Astrophysics Data System.

Facilities: Topcat

REFERENCES

- Agüeros, M. A., Bowsher, E. C., Bochanski, J. J., et al. 2018, *ApJ*, 862, 33
- Allard, F., Hauschildt, P. H., Alexander, D. R., Tamanai, A., & Schweitzer, A. 2001, *ApJ*, 556, 357
- Allard, F., Homeier, D., Freytag, B., & Sharp, C. M. 2012, in *EAS Publications Series*, Vol. 57, *EAS Publications Series*, ed. C. Reylé, C. Charbonnel, & M. Schultheis, 3–43
- An, D., Terndrup, D. M., Pinsonneault, M. H., et al. 2007, *ApJ*, 655, 233
- Anthony-Twarog, B. J., Deliyannis, C. P., Twarog, B. A., Croxall, K. V., & Cummings, J. D. 2009, *AJ*, 138, 1171
- Asplund, M., Grevesse, N., Sauval, A. J., & Scott, P. 2009, *ARA&A*, 47, 481
- Bailey, J. I., Mateo, M., White, R. J., Sheckman, S. A., & Crane, J. D. 2018, *MNRAS*, 475, 1609
- Baraffe, I., Chabrier, G., Allard, F., & Hauschildt, P. H. 2002, *A&A*, 382, 563
- Barrado y Navascués, D., Deliyannis, C. P., & Stauffer, J. R. 2001, *ApJ*, 549, 452
- Barrado y Navascués, D., Stauffer, J. R., & Jayawardhana, R. 2004, *ApJ*, 614, 386
- Barrado y Navascués, D., Stauffer, J. R., & Patten, B. M. 1999a, *ApJL*, 522, L53
- Barrado y Navascués, D., Stauffer, J. R., Song, I., & Caillault, J. P. 1999b, *ApJL*, 520, L123
- Basri, G., Marcy, G. W., & Graham, J. R. 1996, *ApJ*, 458, 600
- Bell, C. P. M., Mamajek, E. E., & Naylor, T. 2015, *MNRAS*, 454, 593
- Bell, C. P. M., Murphy, S. J., & Mamajek, E. E. 2017, *MNRAS*, 468, 1198
- Bell, C. P. M., Naylor, T., Mayne, N. J., Jeffries, R. D., & Littlefair, S. P. 2013, *MNRAS*, 434, 806
- Bell, C. P. M., Rees, J. M., Naylor, T., et al. 2014, *MNRAS*, 445, 3496
- Bildsten, L., Brown, E. F., Matzner, C. D., & Ushomirsky, G. 1997, *ApJ*, 482, 442
- Binks, A. S., & Jeffries, R. D. 2014, *MNRAS*, 438, L11
- Binks, A. S., Jeffries, R. D., Jackson, R. J., et al. 2021, *MNRAS*, 505, 1280
- Blanco-Cuaresma, S., Soubiran, C., Heiter, U., & Jofré, P. 2014, *A&A*, 569, A111
- Böcek Topcu, G., Afşar, M., Sneden, C., et al. 2020, *MNRAS*, 491, 544
- Boesgaard, A. M., & Friel, E. D. 1990, *ApJ*, 351, 467
- Bossini, D., Vallenari, A., Bragaglia, A., et al. 2019, *A&A*, 623, A108
- Boudreault, S., Bailer-Jones, C. A. L., Goldman, B., Henning, T., & Caballero, J. A. 2010, *A&A*, 510, A27
- Bragaglia, A., Alfaro, E. J., Flaccomio, E., et al. 2022, *A&A*, 659, A200
- Brandner, W., Calissendorff, P., & Kopytova, T. 2023a, *AJ*, 165, 108
- . 2023b, *arXiv e-prints*, arXiv:2306.03132
- . 2023c, *MNRAS*, 518, 662
- Brandt, T. D., & Huang, C. X. 2015, *ApJ*, 807, 58
- Bressan, A., Marigo, P., Girardi, L., et al. 2012, *MNRAS*, 427, 127
- Buder, S., Sharma, S., Kos, J., et al. 2021, *MNRAS*, 506, 150
- Burke, C. J., Pinsonneault, M. H., & Sills, A. 2004, *ApJ*, 604, 272
- Cantat-Gaudin, T., Anders, F., Castro-Ginard, A., et al. 2020, *A&A*, 640, A1
- Capitanio, L., Lallement, R., Vergely, J. L., Elyajouri, M., & Monreal-Ibero, A. 2017, *A&A*, 606, A65
- Cardelli, J. A., Clayton, G. C., & Mathis, J. S. 1989, *ApJ*, 345, 245

- Cargile, P. A., James, D. J., & Jeffries, R. D. 2010, *ApJL*, 725, L111
- Cargile, P. A., James, D. J., Pepper, J., et al. 2014, *ApJ*, 782, 29
- Carrera, R., & Pancino, E. 2011, *A&A*, 535, A30
- Casamiquela, L., Soubiran, C., Jofré, P., et al. 2021, *A&A*, 652, A25
- Castellani, V., Degl'Innocenti, S., & Prada Moroni, P. G. 2001, *MNRAS*, 320, 66
- Castelli, F., & Kurucz, R. L. 2003, in *Modelling of Stellar Atmospheres*, ed. N. Piskunov, W. W. Weiss, & D. F. Gray, Vol. 210, A20
- Chen, Y., Bressan, A., Girardi, L., et al. 2015, *MNRAS*, 452, 1068
- Chen, Y., Girardi, L., Bressan, A., et al. 2014, *MNRAS*, 444, 2525
- Chen, Y., Girardi, L., Fu, X., et al. 2019, *A&A*, 632, A105
- Choi, J., Dotter, A., Conroy, C., et al. 2016, *ApJ*, 823, 102
- Claria, J. J. 1982, *A&AS*, 47, 323
- Cordoni, G., Milone, A. P., Marino, A. F., et al. 2023, *A&A*, 672, A29
- Costa, G., Girardi, L., Bressan, A., et al. 2019, *MNRAS*, 485, 4641
- Cummings, J. D., Deliyannis, C. P., Anthony-Twarog, B., Twarog, B., & Maderak, R. M. 2012, *AJ*, 144, 137
- Da Rio, N., Gouliermis, D. A., & Gennaro, M. 2010, *ApJ*, 723, 166
- Dahm, S. E. 2015, *ApJ*, 813, 108
- Daniel, S. A., Latham, D. W., Mathieu, R. D., & Twarog, B. A. 1994, *PASP*, 106, 281
- D'Antona, F., & Mazzitelli, I. 1994, *ApJS*, 90, 467
- De Gennaro, S., von Hippel, T., Jefferys, W. H., et al. 2009, *ApJ*, 696, 12
- Dias, W. S., Alessi, B. S., Moitinho, A., & Lépine, J. R. D. 2002, *A&A*, 389, 871
- Dias, W. S., Monteiro, H., Moitinho, A., et al. 2021, *MNRAS*, 504, 356
- Dobbie, P. D., Lodieu, N., & Sharp, R. G. 2010, *MNRAS*, 409, 1002
- Dotter, A. 2016, *ApJS*, 222, 8
- Eggen, O. J. 1998, *AJ*, 116, 284
- Evans, D. W., Riello, M., De Angeli, F., et al. 2018, *A&A*, 616, A4
- Feiden, G. A. 2016, *A&A*, 593, A99
- Ford, A., Jeffries, R. D., & Smalley, B. 2005, *MNRAS*, 364, 272
- Fritzewski, D. J., Barnes, S. A., James, D. J., et al. 2019, *A&A*, 622, A110
- Fu, X., Bressan, A., Molaro, P., & Marigo, P. 2015, *MNRAS*, 452, 3256
- Fu, X., Bragaglia, A., Liu, C., et al. 2022, *A&A*, 668, A4
- Gagné, J., Mamajek, E. E., Malo, L., et al. 2018, *ApJ*, 856, 23
- Gaia Collaboration, Babusiaux, C., van Leeuwen, F., et al. 2018, *A&A*, 616, A10
- Gaia Collaboration, Vallenari, A., Brown, A. G. A., et al. 2023, *A&A*, 674, A1
- Galli, P. A. B., Miret-Roig, N., Bouy, H., Olivares, J., & Barrado, D. 2023, *MNRAS*, 520, 6245
- Gebran, M., & Monier, R. 2008, *A&A*, 483, 567
- Gebran, M., Vick, M., Monier, R., & Fossati, L. 2010, *A&A*, 523, A71
- Girardi, L., Costa, G., Chen, Y., et al. 2019, *MNRAS*, 488, 696
- Godoy-Rivera, D., Pinsonneault, M. H., & Rebull, L. M. 2021, *ApJS*, 257, 46
- Groenewegen, M. A. T., Decin, L., Salaris, M., & De Cat, P. 2007, *A&A*, 463, 579
- Hauschildt, P. H., Allard, F., & Baron, E. 1999a, *ApJ*, 512, 377
- Hauschildt, P. H., Allard, F., Ferguson, J., Baron, E., & Alexander, D. R. 1999b, *ApJ*, 525, 871
- Herczeg, G. J., & Hillenbrand, L. A. 2015, *ApJ*, 808, 23
- Hünsch, M., & Weidner, C. 2003, in *Cambridge Workshop on Cool Stars, Stellar Systems, and the Sun*, Vol. 12, *The Future of Cool-Star Astrophysics: 12th Cambridge Workshop on Cool Stars, Stellar Systems, and the Sun*, ed. A. Brown, G. M. Harper, & T. R. Ayres, 787–792
- Hunt, E. L., & Reffert, S. 2024, *arXiv e-prints*, arXiv:2403.05143
- Ilin, E., Schmidt, S. J., Poppenhäger, K., et al. 2021, *A&A*, 645, A42
- Jeffries, R. D., Jackson, R. J., & Binks, A. S. 2023a, *MNRAS*, 526, 1260
- Jeffries, R. D., Naylor, T., Mayne, N. J., Bell, C. P. M., & Littlefair, S. P. 2013, *MNRAS*, 434, 2438
- Jeffries, R. D., Naylor, T., Walter, F. M., Pozzo, M. P., & Devey, C. R. 2009, *MNRAS*, 393, 538
- Jeffries, R. D., & Oliveira, J. M. 2005, *MNRAS*, 358, 13
- Jeffries, R. D., Jackson, R. J., Cottaar, M., et al. 2014, *A&A*, 563, A94
- Jeffries, R. D., Jackson, R. J., Franciosini, E., et al. 2017, *MNRAS*, 464, 1456
- Jeffries, R. D., Jackson, R. J., Wright, N. J., et al. 2023b, *MNRAS*, 523, 802
- Juarez, A. J., Cargile, P. A., James, D. J., & Stassun, K. G. 2014, *ApJ*, 795, 143
- Kerr, R., Kraus, A. L., Murphy, S. J., et al. 2022, *ApJ*, 941, 143

- Kharchenko, N. V., Piskunov, A. E., Röser, S., Schilbach, E., & Scholz, R. D. 2005, *A&A*, 438, 1163
- Kharchenko, N. V., Piskunov, A. E., Schilbach, E., Röser, S., & Scholz, R. D. 2013, *A&A*, 558, A53
- King, J. R., Soderblom, D. R., Fischer, D., & Jones, B. F. 2000, *ApJ*, 533, 944
- Kopytova, T. G., Brandner, W., Tognelli, E., et al. 2016, *A&A*, 585, A7
- Kounkel, M., & Covey, K. 2019, *AJ*, 158, 122
- Kraus, A. L., Shkolnik, E. L., Allers, K. N., & Liu, M. C. 2014, *AJ*, 147, 146
- Lallement, R., Vergely, J. L., Valette, B., et al. 2014, *A&A*, 561, A91
- Lallement, R., Capitanio, L., Ruiz-Dern, L., et al. 2018, *A&A*, 616, A132
- Lee, J., Song, I., & Murphy, S. J. 2022, *MNRAS*, 511, 6179
- Lee, R. A., Gaidos, E., van Saders, J., Feiden, G. A., & Gagné, J. 2024, *MNRAS*, 528, 4760
- Li, L., & Shao, Z. 2022, *ApJ*, 930, 44
- Li, L., Shao, Z., Li, Z.-Z., et al. 2020, *ApJ*, 901, 49
- Liu, F., Yong, D., Asplund, M., Ramírez, I., & Meléndez, J. 2016, *MNRAS*, 457, 3934
- Liu, L., & Pang, X. 2019, *ApJS*, 245, 32
- Lodieu, N. 2020, *Mem. Soc. Astron. Italiana*, 91, 84
- Lodieu, N., Pérez-Garrido, A., Smart, R. L., & Silvotti, R. 2019, *A&A*, 628, A66
- Lodieu, N., Rebolo, R., & Pérez-Garrido, A. 2018, *A&A*, 615, L12
- Lum, M. G., & Boesgaard, A. M. 2019, *ApJ*, 878, 99
- Maderak, R. M., Deliyannis, C. P., King, J. R., & Cummings, J. D. 2013, *AJ*, 146, 143
- Magrini, L., Randich, S., Donati, P., et al. 2015, *A&A*, 580, A85
- Malo, L., Doyon, R., Feiden, G. A., et al. 2014, *ApJ*, 792, 37
- Malo, L., Doyon, R., Lafrenière, D., et al. 2013, *ApJ*, 762, 88
- Mamajek, E. E. 2007, in *Triggered Star Formation in a Turbulent ISM*, ed. B. G. Elmegreen & J. Palous, Vol. 237, 442–442
- Mamajek, E. E., & Bell, C. P. M. 2014, *MNRAS*, 445, 2169
- Manzi, S., Randich, S., de Wit, W. J., & Palla, F. 2008, *A&A*, 479, 141
- Martín, E. L., Lodieu, N., Pavlenko, Y., & Béjar, V. J. S. 2018, *ApJ*, 856, 40
- Mazzei, P., & Pigatto, L. 1989, *A&A*, 213, L1
- Mermilliod, J. C. 1981, *A&A*, 97, 235
- Messina, S., Lanzafame, A. C., Feiden, G. A., et al. 2016, *A&A*, 596, A29
- Monroe, T. R., & Pilachowski, C. A. 2010, *AJ*, 140, 2109
- Naylor, T. 2009, *MNRAS*, 399, 432
- Netopil, M., Oralhan, İ. A., Çakmak, H., Michel, R., & Karataş, Y. 2022, *MNRAS*, 509, 421
- Netopil, M., Paurzen, E., Heiter, U., & Soubiran, C. 2016, *A&A*, 585, A150
- Nguyen, C. T., Costa, G., Girardi, L., et al. 2022, *A&A*, 665, A126
- Nisak, A. H., White, R. J., Yep, A., et al. 2022, *AJ*, 163, 278
- Pace, G., Pasquini, L., & François, P. 2008, *A&A*, 489, 403
- Pang, X., Wang, Y., Tang, S.-Y., et al. 2023, *AJ*, 166, 110
- Patenaude, M. 1978, *A&A*, 66, 225
- Paxton, B., Bildsten, L., Dotter, A., et al. 2011, *ApJS*, 192, 3
- Paxton, B., Cantiello, M., Arras, P., et al. 2013, *ApJS*, 208, 4
- Paxton, B., Marchant, P., Schwab, J., et al. 2015, *ApJS*, 220, 15
- Perryman, M. A. C., Brown, A. G. A., Lebreton, Y., et al. 1998, *A&A*, 331, 81
- Pickles, A. J. 1998, *PASP*, 110, 863
- Pietrinferni, A., Cassisi, S., Salaris, M., & Castelli, F. 2004, *ApJ*, 612, 168
- Preibisch, T. 2012, *Research in Astronomy and Astrophysics*, 12, 1
- Rain, M. J., Ahumada, J. A., & Carraro, G. 2021, *A&A*, 650, A67
- Randich, S., Pallavicini, R., Meola, G., Stauffer, J. R., & Balachandran, S. C. 2001a, *A&A*, 372, 862
- . 2001b, *A&A*, 372, 862
- Randich, S., Tognelli, E., Jackson, R., et al. 2018, *A&A*, 612, A99
- Rebolo, R., Martin, E. L., Basri, G., Marcy, G. W., & Zapatero-Osorio, M. R. 1996, *ApJL*, 469, L53
- Reddy, A. B. S., Lambert, D. L., & Giridhar, S. 2016, *MNRAS*, 463, 4366
- Sestito, P., Randich, S., & Pallavicini, R. 2004, *A&A*, 426, 809
- Shkolnik, E. L., Allers, K. N., Kraus, A. L., Liu, M. C., & Flagg, L. 2017, *AJ*, 154, 69
- Siegel, M. H., LaPorte, S. J., Porterfield, B. L., Hagen, L. M. Z., & Gronwall, C. A. 2019, *AJ*, 158, 35
- Soderblom, D. R., Laskar, T., Valenti, J. A., Stauffer, J. R., & Rebull, L. M. 2009, *AJ*, 138, 1292
- Spina, L., Randich, S., Palla, F., et al. 2014, *A&A*, 567, A55
- Spina, L., Ting, Y. S., De Silva, G. M., et al. 2021, *MNRAS*, 503, 3279
- Spoo, T., Tayar, J., Frinchaboy, P. M., et al. 2022, *AJ*, 163, 229
- Stauffer, J. R., Schultz, G., & Kirkpatrick, J. D. 1998, *ApJL*, 499, L199

- Tang, J., Bressan, A., Rosenfield, P., et al. 2014, *MNRAS*, 445, 4287
- Taylor, B. J. 2008, *AJ*, 136, 1388
- Taylor, B. J., & Joner, M. D. 2005, *ApJS*, 159, 100
- Taylor, M. B. 2005, in *Astronomical Society of the Pacific Conference Series*, Vol. 347, *Astronomical Data Analysis Software and Systems XIV*, ed. P. Shopbell, M. Britton, & R. Ebert, 29
- Tognelli, E., Prada Moroni, P. G., & Degl'Innocenti, S. 2011, *A&A*, 533, A109
- Torres, C. A. O., Quast, G. R., Melo, C. H. F., & Sterzik, M. F. 2008, in *Handbook of Star Forming Regions*, Volume II, ed. B. Reipurth, Vol. 5 (Publisher Unknown), 757
- Twarog, B. A., Anthony-Twarog, B. J., & Deliyannis, C. P. 2023, *AJ*, 165, 105
- Ventura, P., Zeppieri, A., Mazzitelli, I., & D'Antona, F. 1998, *A&A*, 331, 1011
- Yang, X. L., Chen, Y. Q., & Zhao, G. 2015, *AJ*, 150, 158
- Yen, S. X., Reffert, S., Schilbach, E., et al. 2018, *VizieR Online Data Catalog*, J/A+A/615/A12
- Zhong, J., Chen, L., Wu, D., et al. 2020, *A&A*, 640, A127

APPENDIX

A. THE METALLICITIES AND AGES FROM LITERATURE FOR HYADES, PLEIADES AND PRAESEPE.

As shown in the table, we show the metallicities $[Fe/H]$ and Ages of Hyades, Pleiades and Praesepe from the literature.

Table A.1. Data from the literature for the Hyades, Pleiades and Praesepe open clusters with metallicies and ages.

Clusters	$[Fe/H]$	R	ref	Age/Myr	method	ref
Hyades	0.28±0.03	1800	1	650±70	LDB	11
	0.05±0.08	1800	2	750±100	LDB	12
	0.135±0.005		3	625±25	iso	13
	0.13±0.02		4	690±160	iso	4
	0.10		5	650±70	LDB	14
	0.11±0.01	30000	6	580–950	iso	15
	0.0±0.02	60000	7	640 ⁺⁶⁷ ₋₄₉	iso	16
	0.13±0.05	≥25000	8	720±130	iso	8
	0.127±0.022		9	500–1000	iso	17
	0.05±0.05		10	648±45	iso	18
	0.12±0.04	25000	56	794 ⁺¹⁶¹ ₋₁₀₂	iso	19
	0.145±0.063	28000	57	650±70	LDB	11
	0.131±0.015		58	794 ⁺¹⁶¹ ₋₁₀₂	iso	19
	Pleiades	0.10±0.002	1800	1	130±20	LDB
0.03±0.04			20	112±5	LDB	28
-0.034±0.024			9	120–130	LDB	29
0.0±0.01			21	135	iso	30 ⁸
0.06±0.05			22	120	iso	31
0.06±0.23			23	≥120	iso	32
0.03±0.02			24	150	iso	33
-0.039±0.014			25	78	iso	34
0.06±0.06			26	50	iso	35
-0.037±0.026			4	135±25	iso	4
-0.01±0.05		≥25000	8	100±40	iso	8
0.0±0.05		25000	56	134 ⁺⁹ ₋₁₀	LDB	36
-0.010±0.049		28000	57	115 ⁺³ ₋₁₁	iso	37
				132±2	iso	38
				86 ⁺⁶ ₋₃	iso	39
				132 ⁺²⁶ ₋₂₇	iso	16
				126±11	LDB	40
				≥1151	LDB	41
				1241	iso	42
			141 ⁺²⁹ ₋₄₁	iso	43	
			135	iso	44	
Praesepe	0.16±0.06		45	750±7	iso	4
	0.08±0.03		46	730±190	iso	8
	0.25±0.003	1800	1	700	iso	42
	0.221±0.084	1800	53	794 ⁺²⁵³ ₋₂₇₀	iso	43
	0.16		4	700	iso	50
0.16±0.05	30000	47	760	iso	51	

Table A.1 continued

⁸ <http://www.univie.ac.at/webda>

Table A.1 (continued)

Clusters	[Fe/H]	R	ref	Age/Myr	method	ref
	0.27±0.10	100000	48	762 ⁺⁶⁴ ₋₅₉	iso	52
	0.11±0.03	55000	49	750	iso	53
	0.16±0.08	≥25000	8	729	iso	54
	0.16±0.07	25000	56	600	iso	55
	0.16		50			
	0.10±0.002		27			
	0.133±0.041	28000	57			
	0.196±0.039		52			
	0.118±0.014		58			

References—1.Fu et al. (2022), 2.Zhong et al. (2020), 3.Cummings et al. (2012), 4.Ilin et al. (2021), 5.Taylor & Jonev (2005), 6.Carrera & Pancino (2011), 7.Liu et al. (2016), 8.Netopil et al. (2016), 9.Boesgaard & Friel (1990), 10.Gebran et al. (2010), 11.Lodieu (2020), 12.Brandt & Huang (2015), 13.Perryman et al. (1998), 14.Martín et al. (2018), 15.Lodieu et al. (2018), 16.Lodieu et al. (2019), 17.Eggen (1998), 18.De Gennaro et al. (2009), 19.Gaia Collaboration et al. (2018), 20.Soderblom et al. (2009), 21.Barrado y Navascués et al. (2001), 22.King et al. (2000), 23.Groenewegen et al. (2007), 24.An et al. (2007), 25.Taylor (2008), 26. Gebran & Monier (2008), 27.Barrado y Navascués et al. (2004), 28.Dahm (2015), 29.Stauffer et al. (1998), 30.Webda database, 31.Kharchenko et al. (2005), 32.Ventura et al. (1998), 33.Mazzei & Pigatto (1989), 34.Mermilliod (1981), 35.Patenaude (1978), 36.Cargile et al. (2014), 37.Naylor (2009), 38.Bell et al. (2014), 39.Bossini et al. (2019), 40.Burke et al. (2004), 41.Basri et al. (1996), 42.Pang et al. (2023), 43.Yen et al. (2018), 44.Kounkel & Covey (2019), 45.Yang et al. (2015), 46.Reddy et al. (2016), 47.Carrera & Pancino (2011), 48.Pace et al. (2008), 49.An et al. (2007), 50.Godoy-Rivera et al. (2021), 51.Cordoni et al. (2023), 52.Dias et al. (2021), 53. Zhong et al. (2020), 54.Dias et al. (2002), 55.Boudreault et al. (2010), 56.Netopil et al. (2022), 57. Spina et al. (2021), 58. Casamiquela et al. (2021)

NOTE—spectral resolution(R), Lithium depletion boundary(LDB); isochrone fitting(iso)

B. ADDITIONAL CMDs FOR THE COLOR CORRECTION OF PLEIADES AND PRAESEPE

Similar to Figure 4 and 5 for Hyades in Section 4, there are CMDs for the color correction of Pleiades and Praesepe.

C. ADDITIONAL INFORMATION OF 31 CLUSTERS AND 3 MOVING GROUPS

In this appendix, we present the CMDs of 30 clusters and 3 moving groups, mentioned in Section 5.1, using the MIST model in Figure C.1 and the PARSEC 1.2S model in Figure C.2.

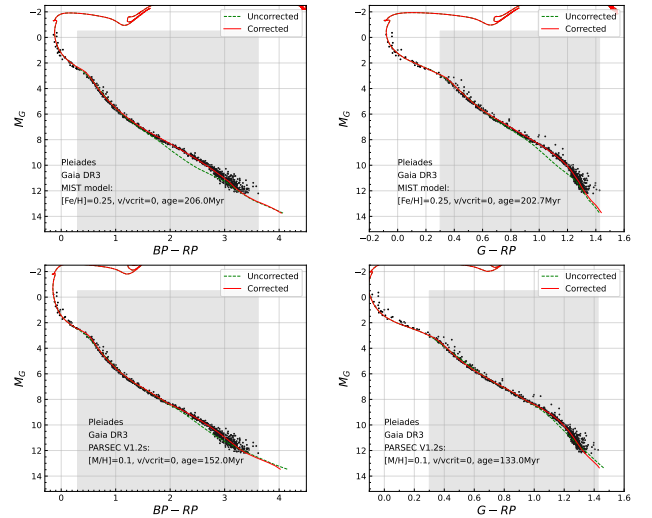


Figure B.1. CMDs of Pleiades open cluster used by MIST model and PARSEC 1.2S model, respectively, similar to Figure 4 and 5.

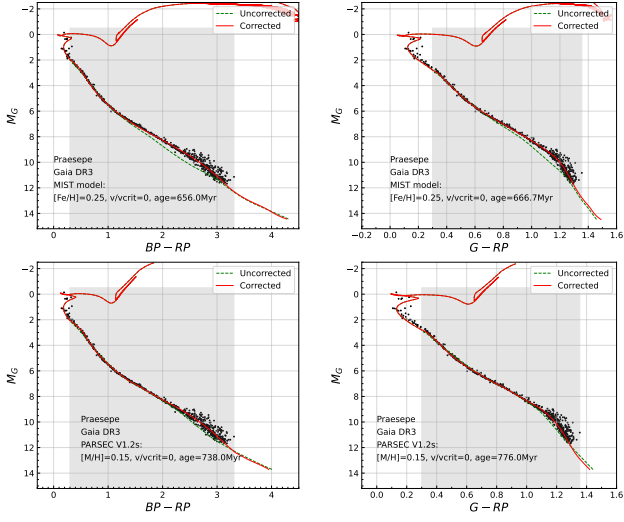


Figure B.2. CMDs of Praesepe open cluster, similar to Figure 4, 5 and B.1.

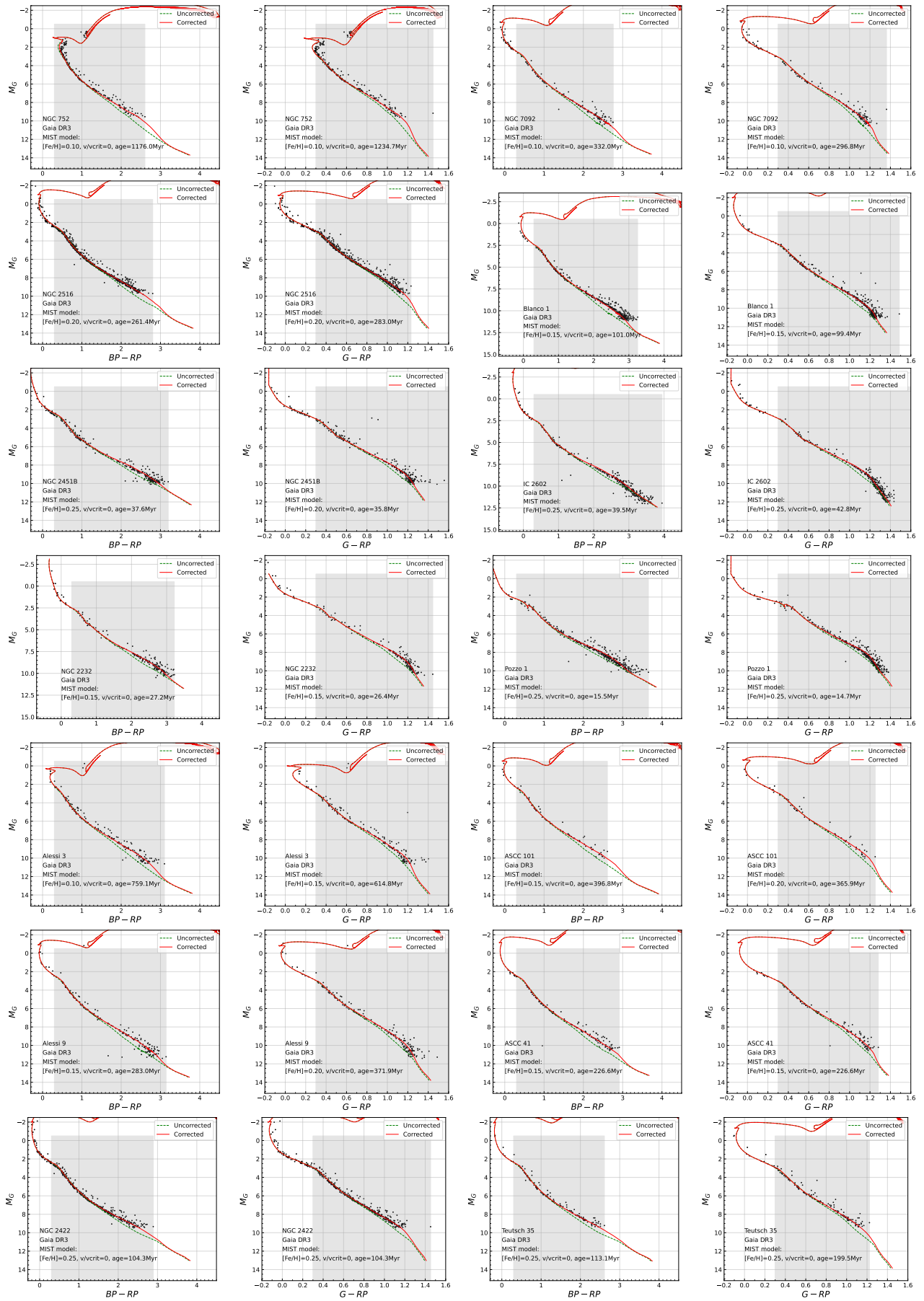


Figure C.1. CMDs of open clusters used by MIST model.

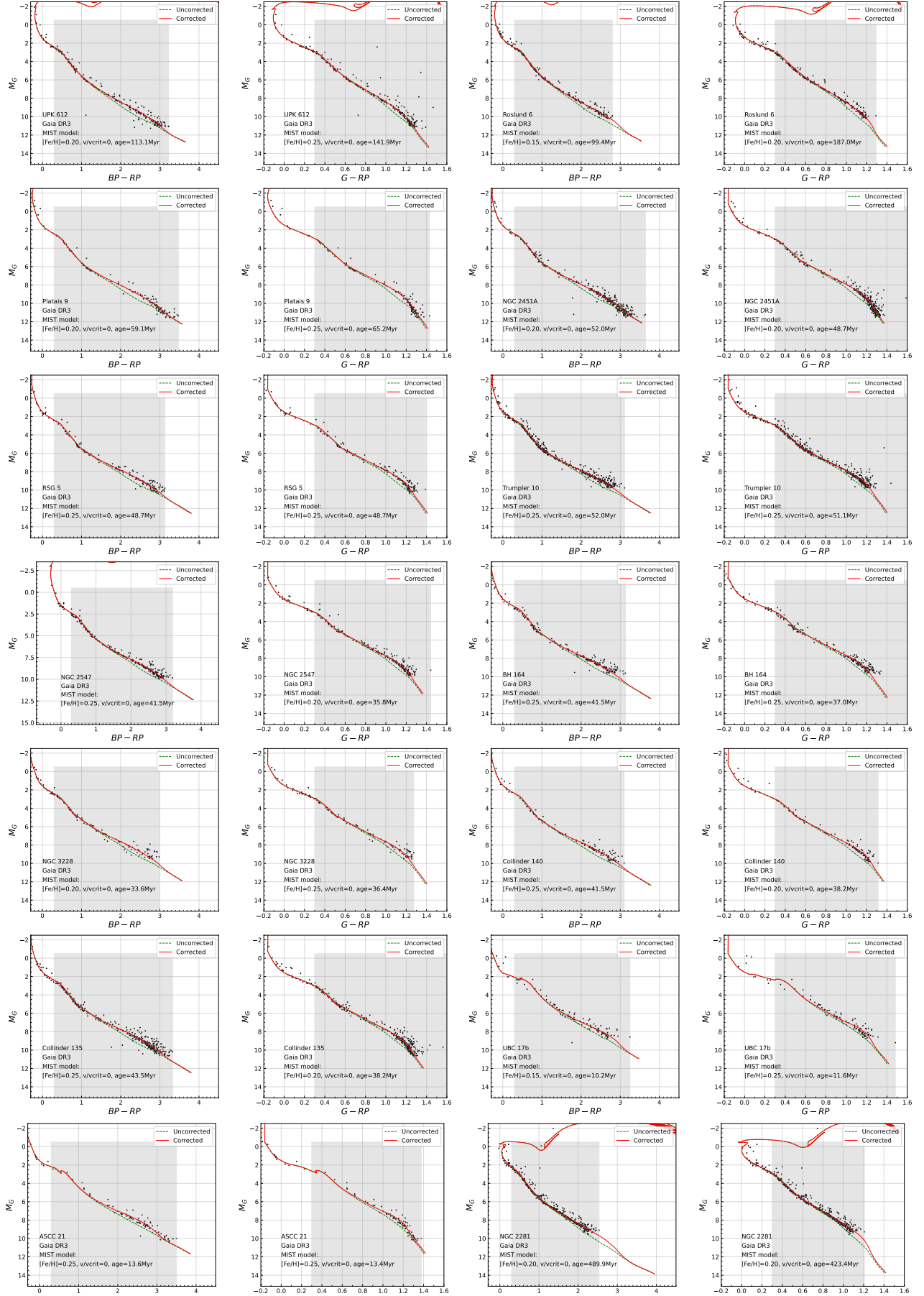


Figure C.1. Continued from Fig C.1

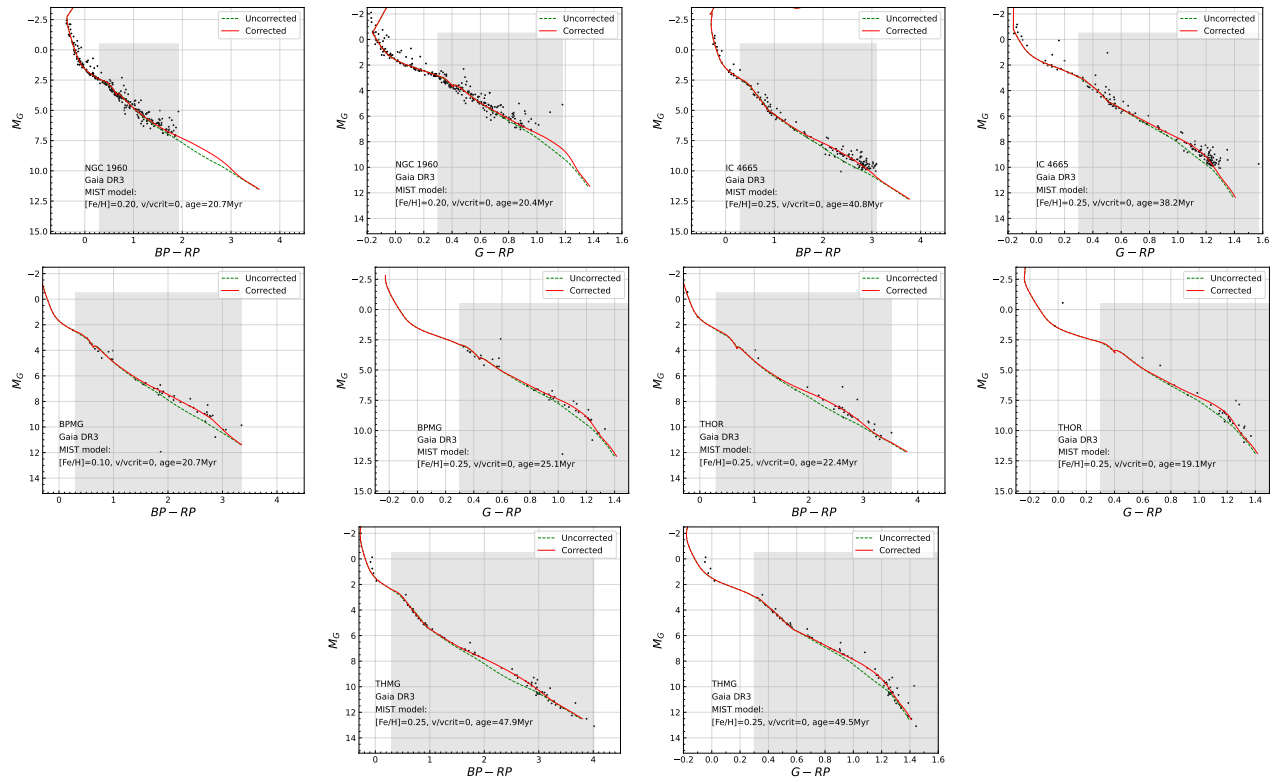


Figure C.1. Continued from Fig C.1

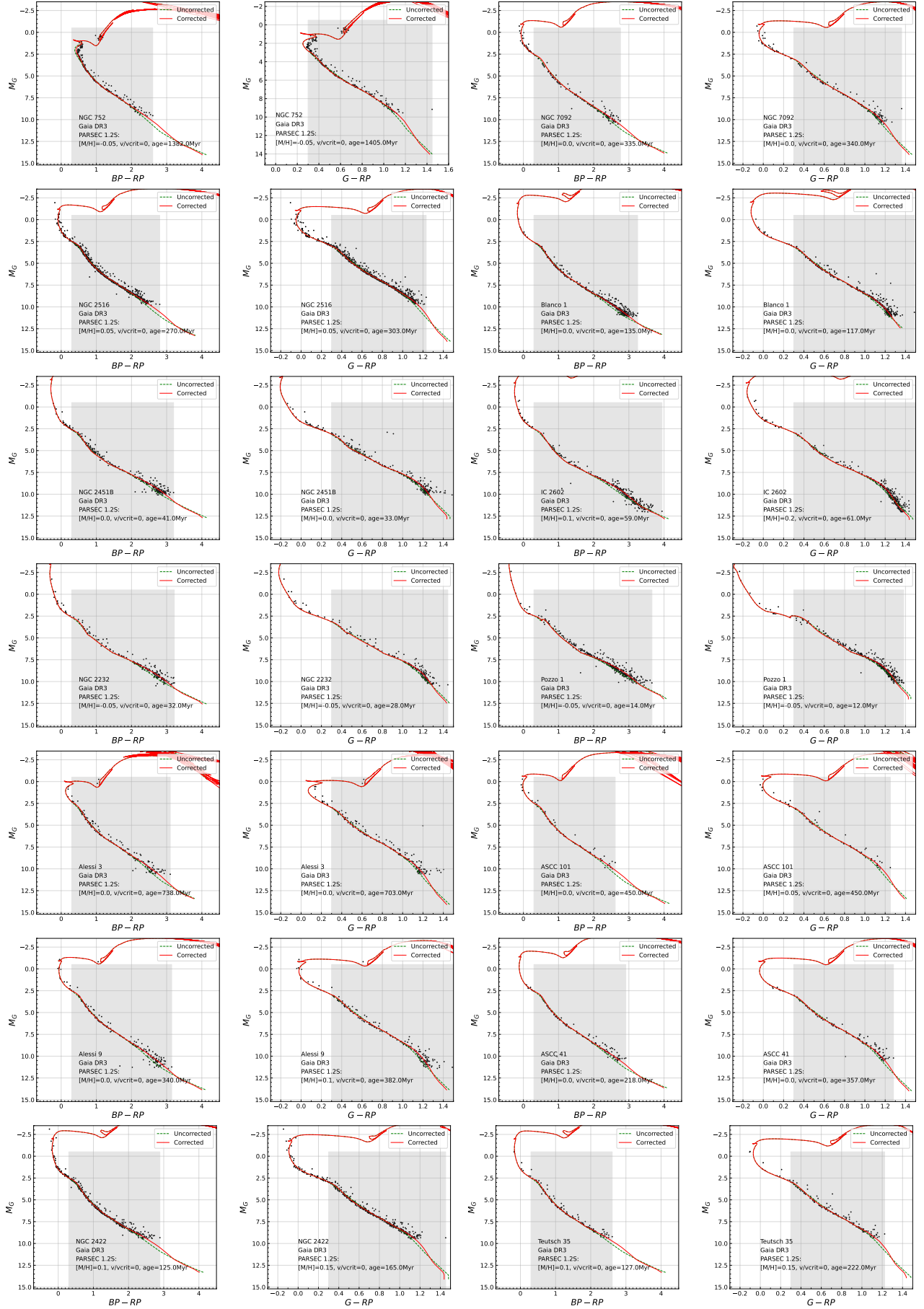


Figure C.2. CMDs of open clusters used by PARSEC 1.2S model.

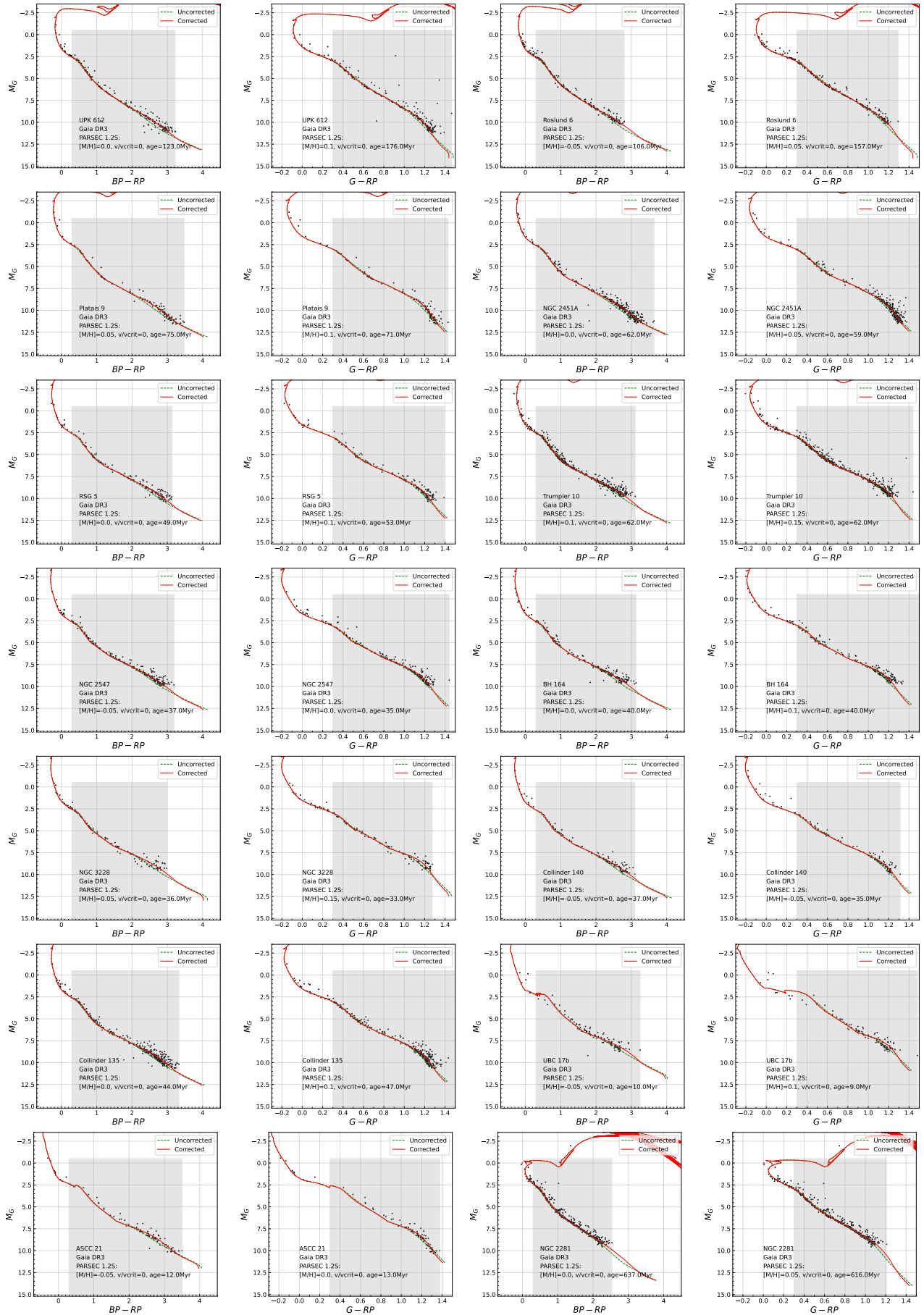


Figure C.2. Continued from Fig C.2

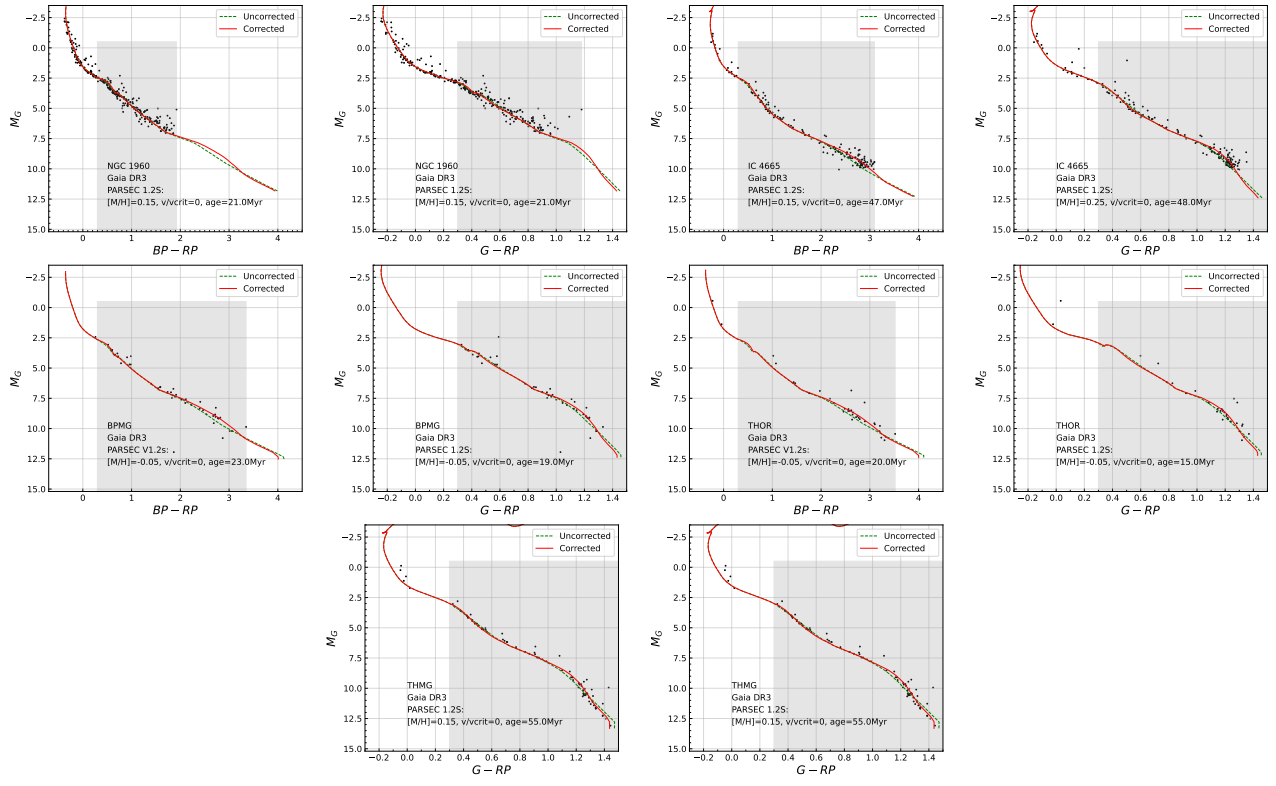


Figure C.2. Continued from Fig C.2

Table C.1. Literature age results for the 31 open clusters and 3 moving groups with isochronal or LDB method. The corresponding $[\text{Fe}/\text{H}]$ results are also listed. For results with the LDB method, the spectral resolution R is listed as well.

Clusters	$[\text{Fe}/\text{H}]$	ref	Age	method	ref
	dex		Myr		
NGC 752	$0.01 \pm 0.04, 0.04 \pm 0.01, -0.063 \pm 0.013, +0.08 \pm 0.04$	1, 3, 5, 7	$\approx 2000, 1340 \pm 60, 1450, 160, 1780, \approx 1413$	L, I, I, I, I, I	2, 4, 6, 7, 9, 10
	$-0.01 \pm 0.06, -0.03 \pm 0.06, -0.064, -0.037 \pm 0.049, -0.082 \pm 0.071$	8, 21, 29, 33, 34	$\approx 1520, 1450 \pm 50, 1175, 1521_{-95}^{+101}, 1247$	I, I, I, I, I	11, 27, 28, 33, 41
	$-0.054 \pm 0.005, -0.04 \pm 0.01, -0.040 \pm 0.007, -0.053 \pm 0.006$	37, 69, 71, 72			
NGC 7092	$-0.047 \pm 0.072, -0.29$	33, 34	$310_{-58}^{+74}, 350, 457_{-61}^{+70}, 501_{-206}^{+74}$	I, I, I, I	17, 30, 33, 39
NGC 2516	$+0.05 \pm 0.11, -0.008 \pm 0.028, +0.05, -0.08 \pm 0.01, 0.1$	21, 33, 39, 43, 66	$123, 277_{-49}^{+60}, 150, 251, 112$	I, I, I, I, I	15, 33, 39, 41, 66
Blanco 1	$+0.04 \pm 0.02, +0.03 \pm 0.07, -0.03, -0.016 \pm 0.023, -0.09 \pm 0.13$	13, 21, 32, 33, 65	$115_{-15}^{+23}, 94_{-7}^{+5}, 146_{-14}^{+13}, 132 \pm 24, 126_{-14}^{+13}$	I, I, I, L, L	15, 17, 22, 23, 24
	$+0.01, +0.04 \pm 0.07, -0.056 \pm 0.048$	66, 69, 71	$105, 103_{-19}^{+24}, 144_{-36}^{+47}, 93.33$	I, I, I, I	32, 33, 40, 66
NGC 2451B	$0.0, -0.02, 0.05 \pm 0.054, +0.06$	21, 32, 33, 66	$39, 50, 41, 47_{-7}^{+7}$	I, I, I, I	17, 30, 32, 33
			$170, 45, 50, 39$	I, I, I, I	35, 36, 38, 66
IC 2602	$-0.05 \pm 0.05, -0.02 \pm 0.02, +0.02 \pm 0.02, -0.06$	14, 21, 31, 32	$40_{-11}^{+10}, 44_{-18}^{+18}, 35.3_{-3}^{+1.3}, 46_{-6}^{+6}$	I, I, I, L	15, 16, 17, 18
	$-0.016 \pm 0.012, -0.02 \pm 0.02, -0.02 \pm 0.05, -0.035 \pm 0.136$	33, 69, 70, 71	$44, 36, 47_{-2.4}^{+2.6}, 100_{-45}^{+12}, 35, 32$	I, I, I, I, I	30, 32, 33, 40, 41, 66
IC 2391	$-0.03 \pm 0.07, -0.01 \pm 0.03, 0.05 \pm 0.02, -0.06$	14, 21, 31, 32	$50 \pm 5, 50_{-13}^{+14}, 36.4 \pm 2.0, 53 \pm 5, 48 \pm 5$	L, I, I, L, L	12, 15, 17, 19, 20
	$0.00 \pm 0.011, +0.03, -0.03 \pm 0.04$	33, 66, 69	$49, 29, 49_{-4.5}^{+5.0}, 81_{-51}^{+118}, 46, 36.31$	I, I, I, I, I	30, 32, 33, 40, 41, 66
NGC 2232	$+0.11, 0.27 \pm 0.08, -0.03, +0.016 \pm 0.06, -0.094 \pm 0.099$	21, 26, 32, 33, 34	$25, 38 \pm 3, 24, 18, 31_{-2.8}^{+3.0}$	I, L, I, I, I	15, 25, 30, 32, 33
	$-0.02 \pm 0.12, +0.03, -0.121 \pm 0.037$	37, 66, 71	$105_{-50}^{+37}, 55, 52.48$	I, I, I	40, 41, 66
Fozzo 1	$-0.069 \pm 0.064, -0.04 \pm 0.05, -0.04 \pm 0.05, +0.07$	33, 61, 62, 66	$15, 12.2_{-2.2}^{+2.7}, 20.0 \pm 4.6, 14$	I, I, I, I	17, 33, 63, 66
Alessi 3	-0.057 ± 0.045	33	$631, 798_{-98}^{+111}, 794_{-163}^{+183}, 637$	I, I, I, I	28, 33, 40, 41
ASCC 101	0.004 ± 0.064	33	$490, 332_{-103}^{+71}, 189$	I, I, I	28, 33, 41
Alessi 9	-0.002 ± 0.050	33	$282, 392_{-60}^{+71}, 291$	I, I, I	28, 33, 41
ASCC 41	$-0.089 \pm 0.056, -0.11 \pm 0.065, -0.08 \pm 0.018$	33, 34, 37	$214, 281_{-113}^{+188}, 100$	I, I, I	28, 33, 41
NGC 2422	$+0.09 \pm 0.03, 0.132 \pm 0.054, -0.05 \pm 0.02, +0.07$	21, 33, 43, 66	$110, 155_{-31}^{+39}, 117, 72.44$	I, I, I, I	28, 33, 41, 66
Teutsch 35	0.078 ± 0.068	33	$103, 231_{-78}^{+103}$	I, I	28, 33
UPK 612	$-0.076 \pm 0.097, +0.021 \pm 0.027$	33, 71	$100, 141_{-50}^{+78}$	I, I	28, 33
Roshund 6	$+0.078 \pm 0.058, -0.010 \pm 0.104, +0.032 \pm 0.011$	33, 34, 37	259_{-41}^{+49}	I	33
Platais 9	-0.025 ± 0.047	33	$50, 56_{-6.9}^{+7.9}, 54$	I, I, I	28, 33, 41
NGC 2451A	$-0.08, +0.050 \pm 0.057, 0.0$	21, 33, 66	$36, 55_{-5.6}^{+6.2}, 148_{-76}^{+98}, 50, 43.65$	I, I, I, I, I	28, 33, 40, 41, 66
RCG 5	$+0.012 \pm 0.076, +0.065 \pm 0.094, 0.105 \pm 0.016$	33, 34, 37	$35, 52_{-4.9}^{+4.9}$	I, I	28, 33
Trumpler 10	$-0.12 \pm 0.06, +0.043 \pm 0.050, +0.03$	21, 33, 66	$33, 57_{-3.3}^{+3.5}, 56, 35$	I, I, I, I	28, 33, 41, 66
NGC 2547	$-0.14 \pm 0.10, -0.014 \pm 0.05, -0.03 \pm 0.06, +0.04, -0.01 \pm 0.01$	21, 33, 64, 66, 68	$33, 39_{-2.1}^{+2.2}, 35, 31, 34.7 \pm 4.0, 27, 57 \pm 5.7$	I, I, I, L, I, I	28, 33, 39, 41, 42, 66, 68
BH 164	-0.002 ± 0.050	33	$33, 46_{-5.7}^{+6.5}$	I, I	28, 33
NGC 3228	$+0.01, +0.143 \pm 0.08$	21, 33	$31, 46_{-6.6}^{+7.7}, 32$	I, I, I	28, 33, 41
Col 140	$+0.01 \pm 0.0, +0.011 \pm 0.04$	21, 33	$27, 40_{-3.3}^{+3.5}$	I, I	28, 33
Col 135	$+0.111 \pm 0.05, +0.03, -0.011 \pm 0.044$	33, 66, 71	$26, 47_{-4.9}^{+5.5}, 47_{-4.9}^{+5.5}$	I, I	28, 66, 33
UBC 17b	$+0.013 \pm 0.012, -0.070 \pm 0.032$	37, 71	12	I	28
ASCC 21	$0.0, -0.008 \pm 0.029, -0.108 \pm 0.318$	17, 33, 34	$11.0 \pm 0.0, -0.03_{-1.1}^{+0.9}, 13_{-1.1}^{+1.2}$	I, I, I	17, 28, 33
NGC 2281	$-0.037 \pm 0.061, -0.085 \pm 0.11, -0.015 \pm 0.007, +0.06$	33, 34, 37, 66	$617, 590_{-77}^{+89}, 590, 354.82$	I, I, I, I	28, 33, 41, 66

Table C.1 continued

Table C.1 (continued)

Clusters	[Fe/H]	ref	Age	method	ref
	dex		Myr		
NGC 1960	-0.030 ± 0.085 , -0.20 ± 0.097 , -0.090 ± 0.025 , $+0.21$	33, 34, 37, 66	$25, 30, 2^{+4.4}_{-3.8}$, 22 ± 4 , $26, 3^{+3.2}_{-5.2}$, 26	I, I, L, I, I	17, 33, 44, 49, 66
IC 4665	-0.03 ± 0.04 , -0.005 ± 0.032 , -0.029 ± 0.011 , $+0.08 \pm 0.015$, $+0.12$	21, 33, 34, 37, 66	38^{+5}_{-2} , 53^{+1}_{-9} , 28 ± 4 , $23, 2^{+3.5}_{-3.1}$, 52^{+8}_{-6}	I, I, L, L, L	17, 33, 45, 46, 47
BPMG	-0.03 ± 0.08 , -0.01 ± 0.02 , -0.034 ± 0.078	67, 69, 71	32^{+4}_{-5} , 38	L, I	48, 66
THOR	-0.01 ± 0.08	17	21 ± 4 , 26 ± 3 , 25 ± 3 , 22 ± 6 , $12 - 22$, 20 ± 10 , 24 ± 3	L, L, L, L, I, I, I	50, 51, 52, 53, 54, 55, 57
THMG	$+0.08 \pm 0.0$	60	23 ± 4 , 22^{+4}_{-3} , 25 ± 2.5	L, I, I	56, 57, 58
			$10 - 40$, 45 ± 4 , 40 ± 3 , 30	I, I, L, I	54, 57, 59, 60

References— 1. Sestito et al. (2004), 2. Sestito et al. (2004), 3. Blanco-Cuadras et al. (2014), 4. Agüeros et al. (2018), 5. Maderak et al. (2013), 6. Anthony-Twarog et al. (2009), 7. Carrera & Pancino (2011), 8. Lum & Boesgaard (2019), 9. Daniel et al. (1994), 10. Siegel et al. (2019), 11. Böcek Topcu et al. (2020), 12. Barrado y Navascués et al. (2004), 13. Ford et al. (2005), 14. Randich et al. (2001a), 15. Gaia Collaboration et al. (2018), 16. Naylor (2009), 17. Bossini et al. (2019), 18. Dobbie et al. (2010), 19. Barrado y Navascués et al. (1999a), 20. Burke et al. (2004), 21. Netopil et al. (2016), 22. Cargile et al. (2014), 23. Cargile et al. (2010), 24. Juárez et al. (2023), 25. Nisak et al. (2021), 26. Monroe & Pilachowski (2010), 27. Twarog et al. (2023), 28. Cantat-Gaudin et al. (2020), 29. Spoo et al. (2022), 30. Pang et al. (2022), 31. Nisak et al. (2022), 32. Bragaglia et al. (2022), 33. Dias et al. (2021), 34. Zhong et al. (2020), 35. Kharchenko et al. (2013), 36. Dias et al. (2002), 37. Fu et al. (2022), 38. Hünsch & Weidner (2003), 39. Godoy-Rivera et al. (2021), 40. Yen et al. (2018), 41. Kounkel & Covey (2019), 42. Jeffries & Oliveira (2005), 43. Bailey et al. (2018), 44. Jeffries et al. (2013), 45. Manzi et al. (2008), 46. Randich et al. (2016), 47. Jeffries et al. (2023b), 48. Jeffries et al. (2023a), 49. Bell et al. (2013), 50. Binks & Jeffries (2014), 51. Malo et al. (2014), 52. Messina et al. (2010), 53. Shkolnik et al. (2017), 54. Malo et al. (2013), 55. Barrado y Navascués et al. (1999b), 56. Bell et al. (2017), 57. Bell et al. (2015), 58. Mamajek (2007), 59. Kraus et al. (2014), 60. Torres et al. (2008), 61. Jeffries et al. (2014), 62. Spina et al. (2014), 63. Jeffries et al. (2009), 64. Magrini et al. (2015), 65. Buder et al. (2021), 66. Rain et al. (2021), 67. Merrifield (1981), 68. Claria (1982), 69. Netopil et al. (2022), 70. Randich et al. (2001b), 71. Spina et al. (2021), 72. Casamiquela et al. (2021)

NOTE—Lithium depletion boundary (LDB, L), isochrone fitting (iso, I).